IEEE Access
Multidisciplinary | Rapid Review | Open Access Journal

Received April 3, 2020, accepted May 2, 2020, date of publication May 7, 2020, date of current version May 20, 2020.

Digital Object Identifier 10.1109/ACCESS.2020.2993056

Distributed Joint Source-Channel Coding-Based Adaptive Dynamic Network Coding

ABDULAH JEZA ALJOHANI[1,2], (Member, IEEE), AND SOON XIN NG[3], (Senior Member, IEEE)

[1]Department of Electrical and Computer Engineering, King Abdulaziz University, Jeddah 21589, Saudi Arabia
[2]Center of Excellence in Intelligent Engineering Systems, King Abdulaziz University, Jeddah 21589, Saudi Arabia
[3]School of Electronics and Computer Science, University of Southampton, Southampton SO17 1BJ, U.K.

Corresponding author: Abdulah Jeza Aljohani (ajaljohani@kau.edu.sa)

This work was supported by the Deanship of Scientific Research (DSR), King Abdulaziz University, Jeddah, under Grant DF-180-135-1441.

ABSTRACT Distributed Source Coding (DSC) schemes rely on separate encoding but joint decoding of statistically dependent sources, which exhibit correlation. More specifically, Distributed Joint Source-Channel coding (DJSC) is associated with the scenario, where the correlated source signals are transmitted through a noisy channel. On one hand, employing DSC or DJSC schemes exploits the existing correlation between sensors resulting in minimising the transmission energy required by the sources, while maintaining reliable communication. On the other hand, Network Coding (NC) is an efficient data transport technique leveraging network efficiency, by allowing Relay Nodes (RNs) in a communication network to combine multiple data packets received via the incoming links before transmitting them to the Destination Node (DN). In this paper, the bandwidth-efficient Distributed Joint Turbo Trellis-Coded Modulation (DJTTCM) aided by both Dynamic Network Coding (DNC) and Adaptive DNC (ADNC)-based cooperative transmission schemes are proposed. Both systems are proposed for supporting correlated source transmissions over hostile channels experiencing both small-scale and large-scale fading in which the RNs dynamically transmit its non-binary linear combinations to the DN. A substantial gain of 19.5 dB was attained at a correlation coefficient of $\rho = 0.8$ over its counterpart dispensing with NC.

INDEX TERMS Distributed source coding, distributed joint source-channel coding, dynamic network coding, Slepian-wolf coding, network coding, joint channel-coding and network-coding, joint channel-coding and network-coding.

LIST OF ABBREVIATIONS

ADNC	Adaptive Dynamic Network Coding
BER	Bit Error Ratio
BP	Broadcast Phase
CP	Cooperative Phase
CSI	Channel State Information
DJSC	Distributed Joint Source-Channel coding
DJSCN	Distributed Joint Source-Channel coding-aided Network-coding
DJTTCM	Distributed Joint Turbo Trellis-Coded Modulation
DN	Destination Node
DNC	Dynamic Network Coding
DSC	Distributed Source Coding
FEC	Forward Error Correction
FER	Frame Error Ratio
GF	Galois Fields
IFs	Information Frames
JCN	Joint Channel-coding and Network-coding
MARCs	Multiple Access Relay Channels
MDS	Maximum Distance Separable
ML	Maximum Likelihood
MUD	Multi-User Detector
NC	Network Coding
PFs	Parity Frames
RNs	Relay Nodes
RS	Reed Solomon
SD	Source-to-Destination
SR	Source-to-Relay
SDMA	Space-Division Multiple Access
SNR	Signal-to-Noise Ratio
SWC	Slepian-Wolf Coding
WZC	Wyner-Ziv Coding

The associate editor coordinating the review of this manuscript and approving it for publication was Asad Waqar Malik.

I. INTRODUCTION

Distributed Source Coding (DSC) refers to the problem of compressing several physically separated, but correlated sources, which are unable to communicate with each other by exploiting that the receiver can perform joint decoding of the encoded signals [1]–[3]. However, Distributed Joint Source-Channel coding (DJSC) is specific to the case, when the correlated sources signals are transmitted over noisy channels [3]–[5]. For both DSC and DJSC schemes the ultimate goal is to exploit the existing correlation for the sake of minimising the transmission energy required by the sources, while maintaining reliable communication. The Slepian-Wolf (SW) theorem [1] has laid down the theoretical foundations of DSC through specifying the achievable rate regions of the compressed correlated sources. Let us consider the arrangement of Fig. 1, where both $\{b_1\}$ and $\{b_2\}$ are random sequences of independent and identically distributed (i.i.d) samples, while R_1 and R_2 are the transmission rates of 1st and 2nd users, respectively. Upon their separate encoding and joint decoding, the SW theorem [1] states the rate region as:

$$R_1 \geq H(b_1|b_2), \tag{1}$$

$$R_2 \geq H(b_2|b_1), \tag{2}$$

$$R_1 + R_2 \geq H(b_1, b_2), \tag{3}$$

where $H(b_1|b_2)$ and $H(b_1, b_2)$ denote the conditional and joint entropies, respectively. Remarkably, and as shown in Fig. 2 this bound is identical regardless of whether joint encoding takes place at the SNs or not. Note that at the corner points shown in Fig. 2, namely A and B, the Slepian-Wolf Coding (SWC) problem would be reduced to the scenario relying on perfect side-information. Using conventional lossless coding at a rate of $R_2 = H(b_2)$, for example, will make $\{b_2\}$ available at the joint decoder, thus approaching point A.

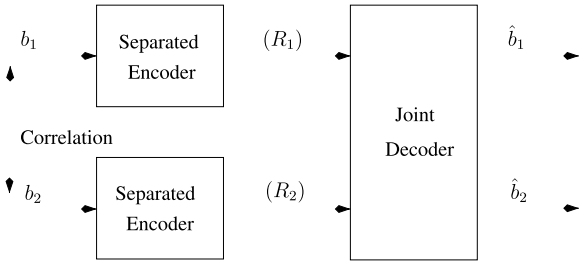

FIGURE 1. Schematic diagram of dispensing with perfect side-information DSC.

Later in 1976, the aforementioned lossless SWC problem of [1] was extended to a lossy source coding problem relying on side-information at the decoder [6], which is widely known as the Wyner-Ziv Coding (WZC) problem [2], [4]. More explicitly, the WZC problem asks the question of how many bits are required for encoding $\{b_1\}$, when the side-information $\{b_2\}$ is perfectly known at the decoder, while maintaining a specific level of distortion concerning $\{b_1\}$ at the receiver. These promising theoretical results have led to

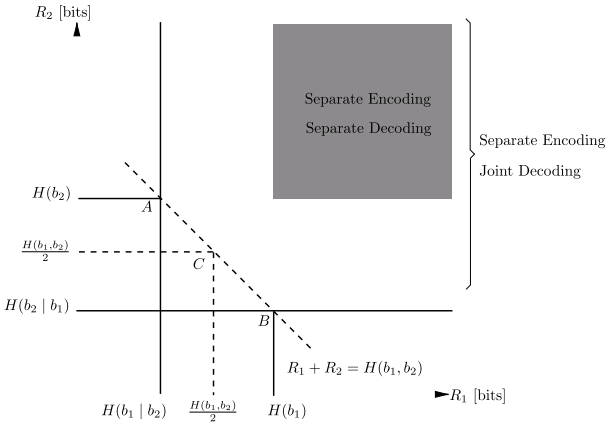

FIGURE 2. Graphical representation of SW bound, using Equations (1)-(3).

intense research activities from both theoretical as well as from practical perspectives.

Both the Network Coding (NC) and DSC schemes have to be carefully designed, when transmitting correlated sources over cooperative networks [7], [8]. More explicitly, the NC would offer multiplexing and/or diversity gains, when communicating over hostile channels, while the DSC scheme would offer source compression by exploiting the correlation between sources. The problem of multi-casting correlated sources over idealised noiseless channel was considered in [9]. Barros *et al.* generalised the problem to correlated sources communicating in a large-scale NC scenario [7]. Inspired by this theoretical contribution, several practical iterative Joint Channel-coding and Network-coding (JCN) schemes have been proposed in [10]–[12], where the NC was combined with channel coding for the sake of achieving time-diversity. The JCN decoder of the schemes advocated in [10]–[12] was based on exchanging soft information between the channel decoder and the network decoder. More explicitly, the channel coding schemes of [10], [11] invoked turbo decoder, while in [12] a Luby Transform-based decoder was employed.

When considering transmissions over a realistic noisy environment, various Distributed Joint Source-Channel coding-aided Network-coding (DJSCN) schemes were investigated in [13]–[16]. To elaborate further, a linear syndrome-based Slepian-Wolf coding assisted random linear NC was proposed in [13]. An iterative receiver that combines a turbo equalizer, a network decoder and a source decoder was proposed in [14], when both sources are communicating over a frequency-selective Rayleigh fading channel. As a further development, a novel iterative turbo code-based DJSCN schemes were proposed in [15] for communicating over orthogonal block Rayleigh fading Multiple Access Relay Channels (MARCs), where the corresponding outage probability was derived in [16]. In contrast to [14], [15], we opted for dispensing with iterative decoding between the NC decoder and the joint decoder in this contribution. This is because of an extremely high complexity would

be imposed, if we extended the scheme of [14], [15] for supporting more than two users. More explicitly, the excessive complexity is mainly imposed by the iterative decoding invoked at the receiver. Additionally, the attainable performance gain when activating such decoding iteration would be limited in the block fading channel environment [17], as the channel coding itself cannot considerably improve the Bit Error Ratio (BER) [18]. Recently, two spatially correlated Markov sources based transmission was supported using DJSC scheme in [19]. Additionally, a novel lattice-based coding algorithm was proposed in [20], which shows a robust transmission over noisy channel. A routing algorithm for multi-hop ad hoc networks-aided DJSC scheme was proposed in [21], in which the wireless network has a significant gain by exploiting the correlation among the sources.

Dynamic Network Coding (DNC) concept was introduced in [22], where each of the Relay Nodes (RN)s dynamically transmits its non-binary linear combinations to the Destination Node (DN). To elaborate further, each of the M users broadcast their Information Frames (IF)s to both the DN and to the RNs during their designated Broadcast Phase (BP). Next, after M BPs, each RN sends its Parity Frames (PFs) to the DN within the Cooperative Phase (CP), where each of these PFs is comprised of non-binary linear combinations of the successfully received IFs. In [23], [24], the DNC techniques were extended, where each of the SNs and RNs is allowed to broadcast its IFs and PFs several times during the BPs and CPs rather than just once as in the DNC counterpart scheme of [22]. In [23], [24], the NC problem was formulated as that of designing a linear Forward Error Correction (FEC) block code, where the diversity order achieved was evaluated in order to quantify the expected performance. The upper and lower Frame Error Ratio (FER) bounds as well as the outage probability of the NC systems was derived in [25].

Adaptive Dynamic Network Coding (ADNC) design was proposed in [17], [26], [27], aiming for enhancing the average transmission rate without degrading the diversity gain of the scheme. A channel-quality feedback flag can be used to indicate, whether the IFs received at the DN were successfully or unsuccessfully decoded during the BPs [17], [26], [27]. As a consequence, the multiplexing gain or the transmission rate can be increased because the number of PFs can be reduced. In [17] an ADNC-based near-capacity irregular convolution code scheme supporting multiple users was proposed, which exhibited an excellent performance when communicating over a hostile environment imposing both fast fading (small-scale uncorrelated Rayleigh fading) and slow fading (quasi-static Rayleigh fading). A novel cooperative cognitive radio aided ADNC regime was proposed in [26] where the cognitive users act as RNs that support the primary users that are the SNs in our case.

Against this background, we intrinsically amalgamate the DJSTTCM scheme of [28] with the Dynamic Network Coding (DNC) of [17], [27], [29], resulting in our proposed scheme referred to as DJSTTCM-DNC.[1] *Additionally, we have also conceived a novel Adaptive Dynamic Network Coding (ADNC) design of for our DJSTTCM scheme, resulting in the DJSTTCM-ADNC regime, where the RNs would adaptively transmit their corresponding frames depending on whether the signal of the sources have been successfully received at the destination or not. Hence, the scheme's overall effective throughput could be enhanced, while the decoding complexity and delay associated with extra frames will be reduced. Both systems, namely DJSTTCM-DNC and DJSTTCM-ADNC, are proposed for supporting correlated source transmissions over hostile channels experiencing both small-scale and large-scale fading. Furthermore, in our NC model the RN signals are composed using non-binary linear coefficients based equations, leading to a further scalability in our design. Note that the NC-based cooperative systems proposed in [14], [15] cannot support more than two users, because the RN signals were constructed using a simple bit-wise XOR operator.*

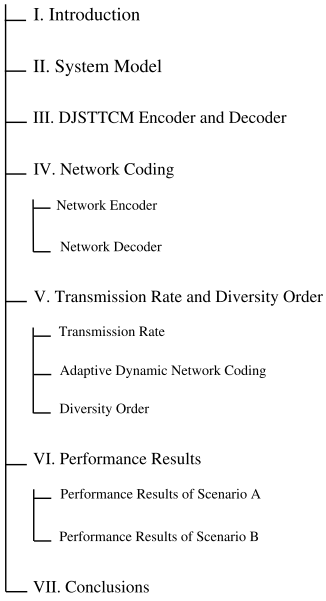

FIGURE 3. Paper structure.

The rest of the paper is organised as seen in Fig. 3. Explicitly, The proposed system model is detailed in Section II, in which the physical layer is explained in Section III followed by the illustrations of the NC encoder and decoder in Section IV. The overall system transmission rate as well as the diversity order are also analysed in Section V. Finally, in Section VI the performance of our proposed scheme is quantified. Finally, our conclusions will be offered in Section VII.

II. SYSTEM MODEL

The schematic of our DJSTTCM-ADNC-based cooperative transmission scheme is shown in Fig. 4, where both the

[1] This paper is related to the unpublished works in Chapter 6 of [30].

correlated SNs, namely SN_1 and SN_2 transmit their data to the DN with the aid of the two RNs.[2] Our communication protocol might be structured into two layers, namely the NC layer and the Forward Error Correction (FEC) layer, where the NC layer is constituted by two transmission sessions, as seen at the upper part of Fig. 4.

More explicitly, the Information Frames (IFs) are broadcast from the corresponding M number of SNs to K RNs as well as to the DN during the Broadcast Phase (BP). Next, the DN decodes the IFs received form the SNs, while the RNs decode the same IFs before encoding them into their corresponding Parity Frames (PFs). Then, PFs are transmitted to the DN during the Cooperative Phase (CP). Thus, as illustrated in Fig. 4, the DN receives the IF that contains the original information during the BP, as well as the PF that comprises a non-binary linear combination of the IFs. The key parameters are defined in Table 1.

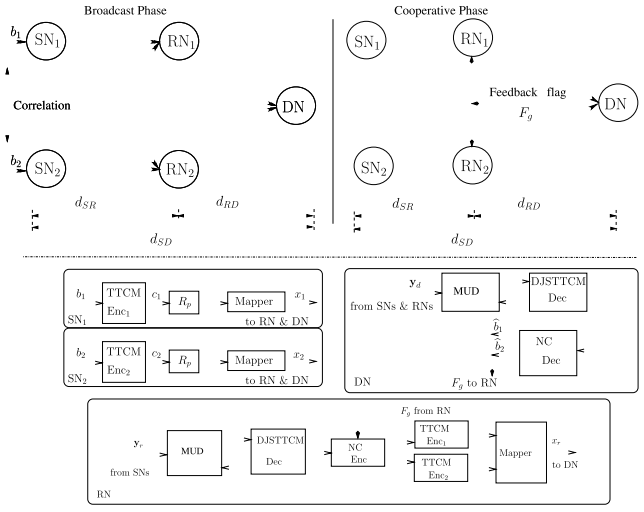

FIGURE 4. Schematic of the DJSTTCM-ADNC transmission, where d_{SD}, d_{SR} and d_{RD} are the geographical distances between $SN_{1,2}$ to DN, $SN_{1,2}$ to $RN_{1,2}$ and $RN_{1,2}$ to DN, respectively, while F_g denotes the feedback flag transmitted from the DN back to the $RN_{1,2}$.

The BP transmission might be viewed as an Space-Division Multiple Access (SDMA) [31] architecture, where M SNs transmit their signals to the RNs, with each RN having equipped with P receive antennas. More specifically, the signal received at the DN via the direct transmission link, namely the Source-to-Destination (SD) link, can be fully characterised using a $(P \times M)$-element channel matrix H_{sd} as:

$$y_d = H_{sd} x_s + n, \tag{4}$$

where $y_d = [y_0, y_1, \cdots, y_{P-1}]^T$ and $n = [n_0, n_1, \cdots, n_{P-1}]^T$ are $(P \times 1)$-element vectors that denote the received signals and noise elements at the DN, respectively. Note that each element in n represents the complex-valued AWGN with a variance of $N_0/2$ per dimension. Additionally, the SNs' transmitted signal $x_s = [x_0, x_1, \cdots, x_{M-1}]^T$ is an $(M \times 1)$-element vector.

This paper considers two main configuration scenarios. The first one is portrayed in the schematic of Fig. 5, where the channel of both phases, namely BP and CP, can be viewed as a (2×2)-elements MIMO MAC. Similar to Equation (4), the signal received at the j^{th} RN via the Source-to-Relay (SR) link can be written as:

$$y_{r_j} = H_{sr_j} x_s + n, \tag{5}$$

where we have $j \in K$ and K is the total number of RNs. Hence, for example, the channel matrix H_{sr_1} of Scenario A seen in Fig. 4 for the SR link during the BP between both

[2]Our proposed scheme has a capability to support more users in a fairly straightforward manner, since both NC decoding and DJSTTCM decoding can be performed separability. Further details will be provided later in Section IV.

TABLE 1. List of symbols.

Parameters	Description
$\{b_1\}$	1^{st} user sequence
$\{b_2\}$	2^{nd} user sequence
R_1 [BPS]	1^{st} user transmission rate
R_2 [BPS]	2^{nd} user transmission rate
$H(b_1\|b_2)$	Conditional entropy
$H(b_1, b_2)$	Joint entropy
R_{cm} [BPS]	TTCM coding rate
R_p [BPS]	Puncturing rate
M [user]	Number of SNs
K [relay]	Number of RNs
F	Total number of simulated frames
N	Total number of bits per simulated frame
N_s	Total number of symbols per frame
i	SN index
j	RN index
n_1 [frame]	# Information Frames (IFs) transmitted per SN during BP within a full transmission cycle
n_2 [frame]	# Parity Frames (PFs) transmitted per transmit antenna per RN during CP within a full transmission cycle
L [antenna]	# transmit antennas of RN
P [antenna]	# receive antennas of RN and DN
$\boldsymbol{G}$	Original transfer matrix that represent the Network Code
$\boldsymbol{G}'$	Modified transfer matrix that represent the Network Code
R_{NC} [BPS]	Network code information rate
R_{FEC} [BPS]	Channel code information rate
$\eta\ [BPS]$	The system overall achievable throughput
D	The diversity order
ρ	Correlation coefficient
α	Path-loss exponent

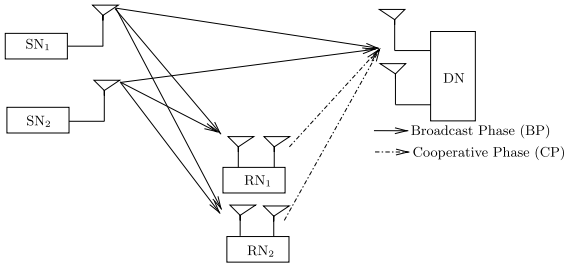

FIGURE 5. Schematic of the cooperative scheme of Scenario A.

SNs and the RN_1 can be expressed as:

$$H_{sr_1} = \begin{bmatrix} \sqrt{G_{s_1r_{1,1}}}\sqrt{P_{tx,s_1}}h_{s_1r_{1,1}} & \sqrt{G_{s_2r_{1,1}}}\sqrt{P_{tx,s_2}}h_{s_2r_{1,1}} \\ \sqrt{G_{s_1r_{1,2}}}\sqrt{P_{tx,s_1}}h_{s_1r_{1,2}} & \sqrt{G_{s_2r_{1,2}}}\sqrt{P_{tx,s_2}}h_{s_2r_{1,2}} \end{bmatrix}, \tag{6}$$

where P_{tx,s_1} and P_{tx,s_2} represent the power transmitted from SN_1 and SN_2, respectively, while $h_{s_1r_{1,l}}$ denotes the channel coefficient between SN_1 and the l^{th} receive antenna of RN_1. Similarly, $G_{s_1r_{1,l}}$ denotes the reduced-pathloss-induced geometrical gain [32] experienced by the SN_1-RN_1 link. As suggested by Fig. 5, the channel corresponding to CP can be expressed in a form similar to Equation (6), albeit, in conjunction with different channel coefficients. For example, assuming a path-loss exponent of two ($\alpha = 2$) i.e. free-space transmission, the corresponding reduced-pathloss-induced geometrical gain experienced by the SR link and RD link with respect to the SD link may be calculated, respectively, as [33], [34]:

$$G_{SR} = \left(\frac{d_{SD}}{d_{SR}}\right)^2; \quad G_{RD} = \left(\frac{d_{SD}}{d_{RD}}\right)^2, \tag{7}$$

where d_{SD} denotes the distance between source nodes SN_1, SN_2 and the DN. The RNs are situated at the mid-point between the SNs and DN. Thus, we have $d_{SR} = d_{RD} = d_{SD}/2$, where $G_{SR} = G_{RD} = 2^2 = 4$.

Without loss of generality, let d_{ab} represent the distance between node a and node b. If x_a is the symbol transmitted from node a equipped with a single transmit antenna, the received Signal-to-Noise Ratio (SNR) estimated at each receive antenna of node b can be expressed as [32]:

$$\begin{aligned} \text{SNR}_r &= \frac{G_{ab}\,\text{E}\left[|h_{ab}|^2\right]\,\text{E}\left[|x_a|^2\right]}{N_0} \\ &= \frac{G_{ab}}{N_0}, \end{aligned} \tag{8}$$

where $\text{E}\left[|h_{ab}|^2\right] = 1$ and $\text{E}\left[|x_a|^2\right] = 1$. We define the transmit SNR[3] as a ratio of the power transmitted from node a to the noise power experienced at the receiver of node b as:

$$\text{SNR}_t = \frac{\text{E}\left[|x_a|^2\right]}{N_0} = \frac{1}{N_0}. \tag{9}$$

[3]However, the concept of transmit SNR [34] is unconventional, as it relates quantities to each other at two physically different locations, namely the transmit power to the noise power at the receiver.

Thus, we arrive at:

$$\begin{aligned} \text{SNR}_r &= \text{SNR}_t\, G_{ab} \\ \Gamma_R &= \Gamma_T + 10\log_{10}(G_{ab})\ [\text{dB}], \end{aligned} \tag{10}$$

where we have $\Gamma_R = 10\log_{10}(\text{SNR}_r)$ and $\Gamma_T = 10\log_{10}(\text{SNR}_t)$.

As stated previously, both the BP and CP transmission channels are composed of two components, with h_s and h_f denoting the uncorrelated fast fading (small-scale Rayleigh fading) and slow fading (quasi-static Rayleigh fading) coefficients, respectively. To elaborate further, each channel coefficient $h_{s_1r_{1,l}}$ of the channel matrix shown in Equation (6) might be expressed as:

$$h = h_s \cdot h_f, \tag{11}$$

where h_s in our simulations is assumed to be constant for all the symbols within a frame, while h_f fluctuates on a symbol by symbol basis within each frame.

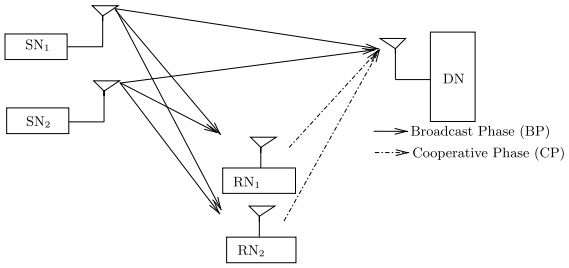

FIGURE 6. Schematic of the cooperative scheme of Scenario B.

In Scenario B of Fig. 6 both the BP and CP may be viewed as (2×1) and (1×1) SDMA channels, respectively. Thus, the channel matrices encountered during both phases can be evaluated similarly to the analysis of Scenario A.

III. DJSTTCM ENCODER AND DECODER

The two correlated sources are encoded using our DJSTTCM [28] encoder and then decoded accordingly. Similar to the source correlation model adopted in [15], [28], [35], [36], the BSC is used for modelling the correlation between the source sequences $\{b_1\} = \{b_1^1, b_1^2, \cdots, b_1^i, \cdots, b_1^N\}$ and $\{b_2\} = \{b_2^1, b_2^2, \cdots, b_2^i, \cdots, b_2^N\}$, where N is the length of each source block. More explicitly, the source sequence $\{b_1\}$ is generated by an equiprobable binary symmetric i.i.d. source, while $\{b_2\}$ can be defined as $b_1^i = b_2^i \oplus e_i$, where $\oplus$ is the modulo-2 addition operation and e_i is an independent binary random variable assuming the logical value 1 with a cross-over probability of p_e and 0 with a probability of $(1 - p_e)$.

The achievable compression rate of both sources is bounded by the SW rate region inequalities of Equations (1)-(3). Both source sequences, namely $\{b_1\}$ and $\{b_2\}$, are first encoded using TTCM encoders having a rate of $R_{cm} = \frac{m}{m+1}$. Then both encoded sequences are mapped onto the corresponding modulated symbols, namely onto

$\{x_1\}$ and $\{x_2\}$, as illustrated in the lower part of Fig. 4. During the BP, both modulated signals are broadcast to all RNs and the DN through either the (2×2) or the (2×1)-element MACs according to the used scenario. Consequently, both received signals, namely y_r and y_d of Fig. 4 are detected by the Maximum Likelihood (ML)-based Multi-User Detector (MUD) at RN and DN, respectively. Then, both source sequences are estimated by iteratively exchanging their extrinsic information between the MUD and the DJSTTCM decoder.

The sequences estimated at the RN will then be fed into the NC before encoding them using a pair of TTCM encoders, as shown in Fig. 4. These TTCM-encoded streams will be transmitted during the CP. Depending on the specific scenario, different mappers or receivers might be used. More explicitly, in Scenario A of Fig. 5, a pair of TTCM-encoded sequences will mapped into two different QPSK signals. However, in Scenario B of Fig. 6, both coded sequences are combined and mapped onto a 16QAM-SPM signal, since the RN and the DN invokes a single receive antenna, as portrayed in Fig. 6.[4]

Before embarking on our NC investigation, we first have to characterise the attainable performance of our DJSTTCM when communicating over the combined uncorrelated Rayleigh fading and quasi-static Rayleigh fading channels of Equation (11). As shown in both Figures 5 and 6, the transmission phases can be characterised in terms of three different channel combinations. In Scenario A of Fig. 5, we have the SD, SR and RD links. More explicitly, the direct transmission might be characterised as a (2×2) MAC regime. Similarly, the SR and SD links of Scenario B of Fig. 6 can be viewed as a (2×1) MAC arrangement, while the RD link can be viewed as a (1×1) channel. More specially, the BER performance of the three channels recorded for various source correlation values is shown in Fig. 7, Fig. 8 and Fig. 9 using the simulation parameters of Table 2. Note that the correlation of the pair of sources is represented by ρ, which is given by $\rho = 1 - 2p_e$, where p_e is the BSC's cross-over probability. As all of these three figures suggested, substantial performance degradation is exhibited once our DJSTTCM scheme [28] encounters a slow fading (quasi-static Rayleigh fading) channel. More specifically, fast Rayleigh fading channel provides useful time diversity that can be explored by channel codes, where each symbol would experience a different fading. However, the slow Rayleigh fading channel does not exhibit this time diversity, since all symbols in a frame would experience the same fading in the slow fading channel. From Equation (11), and when the slow fading factor $|h_s|^2$ is high, the whole frame would enjoy a high receive SNR, where the performance of an uncoded system could be as good as a coded system.

[4] At the RN, although one TTCM would be enough to encode both decoded streams with complexity reduction, we decided to use a couple of TTCM encoders mainly for two reasons. First, to avoid any possible delay when encoding two sequences, second to add further coding flexibility to the design that could be utilised in future works.

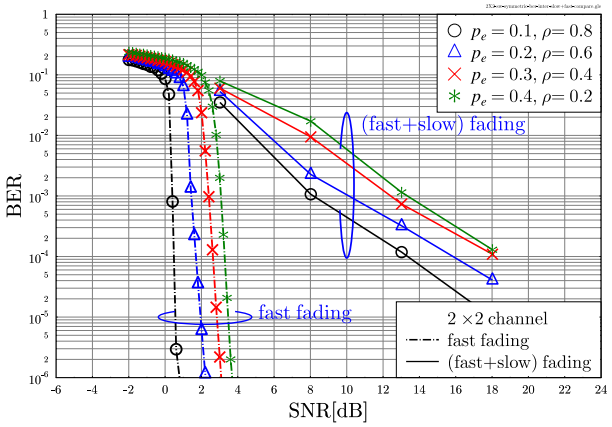

FIGURE 7. BER versus SNR performance of the proposed DJSTTCM-QPSK scheme for correlation coefficients of $\rho = \{0.8, 0.6, 0.4, 0.2\}$, when transmitting over the combined uncorrelated Rayleigh fading and quasi-static Rayleigh fading (2×2) MAC. The main parameters are defined in Table 2, while $R_{FEC} = 2$ BPS.

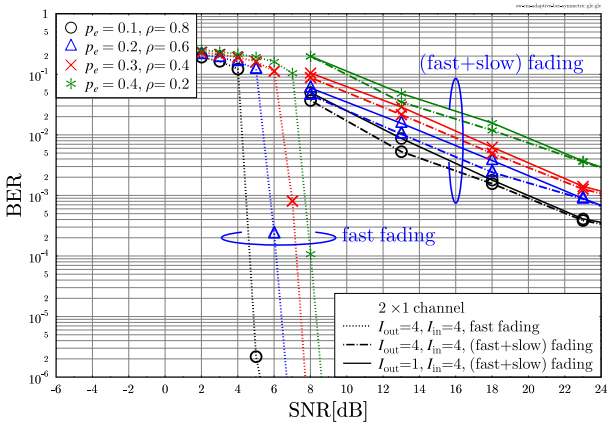

FIGURE 8. BER versus SNR performance of the proposed DJSTTCM-QPSK scheme for correlation coefficients of $\rho = \{0.8, 0.6, 0.4, 0.2\}$ when transmitting over the combined uncorrelated Rayleigh fading and quasi-static Rayleigh fading (2×1) MAC. The main parameters are defined in Table 2, while $R_{FEC} = 2$ BPS.

However when $|h_s|^2$ is low, the SNR for the whole frame could be very poor such that no coding would be able to work properly. Hence, channel coding would not work well in the slow fading channel. In the fast + slow fading scenario, the slow fading factor causes the same issue. More explicitly, the corresponding average received SNR is given by $\frac{\mathrm{E}[|h_f|^2]\mathrm{E}[|h_s|^2]}{N_0} = \frac{|h_s|^2}{N_0}$, where the expectation of both channel is given as $\mathrm{E}\left[|h_f|^2\right] = 1$ and $\mathrm{E}\left[|h_s|^2\right] = |h_s|^2$, respectively.

Fortunately, network coding has been invoked to provide some diversity gains when communicating over slow (or fast + slow) fading channel [24], [37]. Since, the network coding is performed across a few frames, which may have different received SNRs [24], [37].

Quantitatively, Fig. 7 shows the BER versus SNR performance of the DJSTTCM-QPSK scheme, when communicating over the (2×2) MAC regime. Note that the SNR is be given by:

$$\mathrm{SNR[dB]} = E_b/N_0\mathrm{[dB]} + 10\log_{10}(R_{FEC}), \qquad (12)$$

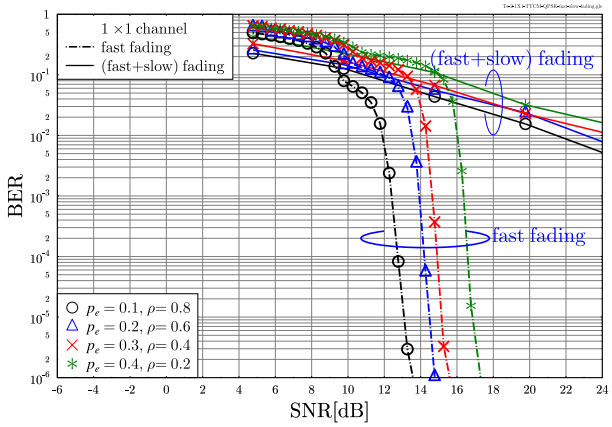

FIGURE 9. BER versus SNR performance of the proposed DJSTTCM-16QAM-SPM scheme for correlation coefficients of $\rho = \{0.8, 0.6, 0.4, 0.2\}$ when transmitting over the combined uncorrelated Rayleigh fading and quasi-static Rayleigh fading (1 × 1) channel. The main parameters are defined in Table 2, $R_{FEC} = 3$ BPS.

TABLE 2. Simulation parameters for the direct link transmission.

Coded Modulation	TTCM
Code rate	$R_{cm} = 1/2$
Correlation coefficients	$\rho = \{0.8, 0.6, 0.4, 0.2\}$
Puncturing rate	$R_p = 1$
Decoding algorithm	Approximated Log-MAP
Inner Iteration	$I_{\text{in}} = 4$
Outer Iteration	$I_{\text{out}} = 4$
Number of symbol	$N_s = 120\,000$ symbols per frame
Number of frames	$F = 10\,000$
Channel	$h_s \cdot h_f$
Channel State Information (CSI)	Known
MUD Type	Maximum Likelihood (ML)

where R_{FEC} denotes the effective channel coding rate that can be expressed as:

$$R_{FEC} = R_{cm} \cdot R_p \cdot \log_2(\mathcal{M}) \cdot M, \tag{13}$$

where $2^{m+1} = \mathcal{M}$ denotes the number of PSK/QAM modulation levels, while M is the number of SNs. As portrayed in Fig. 7, there is an approximately 12.0 dB performance degradation, when the DJSTTCM-QPSK scheme operates over the combined channel compared to that, when transmitting over uncorrelated fading channels. More explicitly, for $\rho = 0.8$ and at a BER level of 10^{-4} an SNR gap of $13 - 0.5 = 12.5$ dB, as seen in Fig. 7. Interestingly, our joint decoder remains capable of exploiting the correlation among the sources, even when communicating over this hostile shadow-faded and fast-faded channel. For example, at a BER of 10^{-4} a considerable 3.0 dB improvement can be attained upon comparing the system having $\rho = 0.8$ to that having $\rho = \{0.6\}$.

As expected, the BER performance was further degraded for the other two channel configurations, namely where the number of the transmit or receive antennas has been reduced to (2×1) and (1×1) channels, as seen in Figures 8 and 9, respectively. To elaborate further, upon analysing Fig. 8 we observe that the DJSTTCM-QPSK scheme requires an excessive transmit power of SNR $= \{19, 22, 24\}$ dB for attaining a BER of 10^{-3} for $\rho = \{0.8, 0.6, 0.4\}$ when the correlated sources encounter the (2×1) channel. Additionally, as it is shown in Fig. 9 for the (1×1) channel, even assigning a transmit power of SNR $= 30$ dB is insufficient for the DJSTTCM-16QAM-SPM scheme to attain a BER $= 10^{-3}$, despite having high correlation value of $\rho = 0.8$. This is not unexpected, because it was pointed out in [18] that in the quasi-static Rayleigh fading channels, the channel coefficients remain constant during the entire transmitted frame, hence for every transmit frame the channel can be viewed as an AWGN channel, albeit, each having different SNR value. More explicitly, the frames associated with low SNRs will dominate the system's performance during the iterative detection process, hence leading to poor mutual information exchange between the constituent decoders. It was found in [16], [17], [38] that network-coded cooperative transmission constitutes an efficient remedy for such a transmission environment, as the time diversity between the frames will be utilised. Let us now discuss the NC scheme in the following sections.

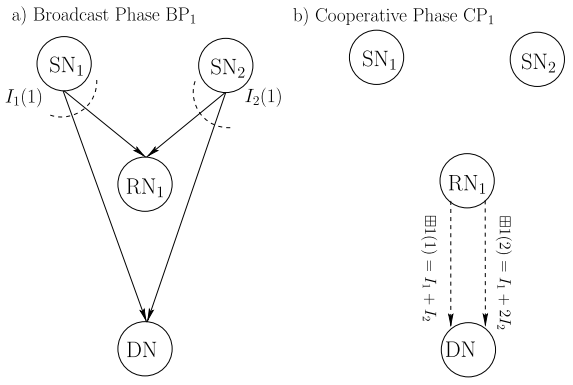

FIGURE 10. Schematic model of an NC-aided system having $M = 2$ SNs transmitting two IFs during the $n_1 = 1$ BP, where the $K = 1$ RN transmit two PFs during the $n_2 = 1$ CP. Table 1 defines the main parameters. The two PFs transmitted during the CP_1, namely ⊞1(1) and ⊞1(2), are generated according to the 3rd and 4th columns of $G_{2\times4}$ respectively, as specified by Equation (14).

IV. NETWORK CODING

Let us consider the NC transmission example illustrated in Fig. 10, where $M = 2$ SNs aim for transmitting their information to the DN with the aid of $K = 1$ RN. In line with [17], [26], [38], NC typically adopts a TDMA-based access method, where each SN broadcasts $n_1 = 1$ IF during its corresponding BP, while each RN transmits $n_1 = 1$ PF

within the CP. Thus, a total of $(n_1 \cdot M + n_2 \cdot K) = 4$ transmission phases are required for accomplishing a full transmission cycle. However, in our SDMA based method, each of the SNs broadcasts $n_1 = 1$ IFs during each BP. Then, during the CP each of the $L = 2$ transmits antennas of the RN transmit $n_2 = 1$ PF, as seen in Fig. 10. More explicitly, both PFs are transmitted using twin-antenna-aided RN when Scenario A of Fig. 5 is invoked. However, for Scenario B of Fig. 6 both of the PFs are combined into a super constellation, creating a single SPM signal as illustrated in [28].

A. NETWORK ENCODER

The NC transmission protocol can be fully characterised using a transfer generator matrix $\boldsymbol{G}$, which is constructed over a Galois Field (GF) (q), where $q = 2^b$ is the desired alphabet size and b is a non-zero integer [22], [38]. In our work, we consider two NC systems relying on the generator matrices of $\boldsymbol{G}_{2\times4}$ and $\boldsymbol{G}_{4\times8}$, where both matrices are generated using the software application SAGE [39]. Upon successfully decoding all of the frames during transmission sessions, $\boldsymbol{G}_{2\times4}$ used in our example of Fig. 10 is given by [22], [37], [40]:

$$\boldsymbol{G}_{2\times4} = \left[\begin{array}{cc|cc} 1 & 0 & 1 & 1 \\ 0 & 1 & 1 & 2 \end{array}\right], \tag{14}$$

where the role of the elements is detailed below. Upon comparing the above transfer matrix to Fig. 10, the transmission arrangement can be characterised by:

$$(BP_1): SN_1 \xrightarrow[(=0 \mid 1)]{I_1(1)} DN, \quad SN_1 \xrightarrow[(=0 \mid 1)]{I_1(1)} RN_1 \tag{15}$$

$$(BP_1): SN_2 \xrightarrow[(=0 \mid 1)]{I_2(1)} DN, \quad SN_2 \xrightarrow[(=0 \mid 1)]{I_2(1)} RN_1 \tag{16}$$

$$(CP_1): RN_1^1 \xrightarrow[(=0 \mid 1)]{\boxplus 1(1)=G(1,3)\cdot I_1+G(2,3)\cdot I_2} DN, \tag{17}$$

$$RN_1^2 \xrightarrow[(=0 \mid 1)]{\boxplus 1(2)=G(1,4)\cdot I_1+G(2,4)\cdot I_2} DN, \tag{18}$$

as detailed below. As seen in Equation (14), $\boldsymbol{G}_{2\times4}$ can be divided into two main parts. The left-hand identity sub-matrix, having diagonal elements of $\boldsymbol{G}_{2\times4}(i,i) = 1$, $i \in \{1,2\}$ represents the transmission of the IFs I_i from the i^{th} SN to the DN during the BP. This phase can be interpreted using Equation (15) and Equation (16), in which the arrow's subscript $(= 0 \mid 1)$ indicates the failure or success of decoding the IFs, respectively. Additionally, the PF construction can be gleaned from the right-hand sub-matrix of $\boldsymbol{G}_{2\times4}$ in Equation (14). More explicitly, each of the signal $\boxplus(1)$ and $\boxplus(2)$[5] that is transmitted from the first and second antennas of RN_1 seen in Fig. 10 are generated according to the 3rd and 4th columns of $\boldsymbol{G}_{2\times4}$, respectively, as specified by Equation (18).

Subsequently, a modified transfer matrix, $\boldsymbol{G}'_{2\times4}$, has to be defined at the DN as justified below. As the terminology *modified* suggests, the entries of $\boldsymbol{G}'_{2\times4}$ are modified according to the success or failure of the transmitted frame. The notation $(= 0)'$ (or $(= 1)'$) beneath the arrows of Equations (15) - (18) indicate, whether the frame was unsuccessfully (or successfully) decoded. Hence, we have $\boldsymbol{G}'_{2\times4} = \boldsymbol{G}_{2\times4}$ when all of the transmitted frames were successfully decoded during both phases. More explicitly, the elements $\boldsymbol{G'}_{2\times4}(i,i) = 1$, $i = [1,2]$ represents the successful decoding of the IFs $I_i(1)$ transmitted by SN_i at the DN during the BP_1. Meanwhile, having $\boldsymbol{G'}_{2\times4}(1,3) =$ "1" or $(\boldsymbol{G'}_{2\times4}(2,4) =$ "2") indicates that the PFs transmitted by the RN during CP_1 are successfully decoded at the DN corresponding to linear combining coefficient of the information frame $I_1(1)$ or $(I_2(2))$. Furthermore, $\boldsymbol{G'}_{2\times4}(2,3) =$ "1" or $(\boldsymbol{G'}_{2\times4}(1,4) =$ "1") signifies that information frame $I_2(2)$ or $(I_1(1))$ is successfully decoded by RN during BP_1, and the PFs transmitted by the RN during the cooperative phase CP_1 are successfully decoded at the DN.

To elaborate further, consider the aforementioned system that might experience an actual transmission scenario, where depending on the success or the failure of each specific transmission attempt we arrive at:

$$(BP_1): \; SN_1 \xrightarrow[(=0)]{I_1(1)} DN \; \boldsymbol{G'}_{2\times4}(1,1) = 0 \tag{19}$$

$$SN_1 \xrightarrow[(=1)]{I_1(1)} RN_1 :: \boldsymbol{G'}_{2\times4}(2,3) = \boldsymbol{G}_{2\times4}(2,3), \tag{20}$$

$$(BP_1): \; SN_2 \xrightarrow[(=0)]{I_2(1)} DN \; \boldsymbol{G'}_{2\times4}(2,2) = 0 \tag{21}$$

$$SN_2 \xrightarrow[(=1)]{I_2(1)} RN_1 : \boldsymbol{G'}_{2\times4}(1,4) = \boldsymbol{G}_{2\times4}(1,4), \tag{22}$$

$$(CP_1): \; RN_1^1 \xrightarrow[(=0)]{\boxplus 1(1)} DN : \boldsymbol{G'}_{2\times4}(i,3) = 0, \quad i = [1,2] \tag{23}$$

$$RN_1^2 \xrightarrow[(=1)]{\boxplus 1(2)} DN : \boldsymbol{G'}_{2\times4}(i,4) = \boldsymbol{G}_{2\times4}(i,4), \quad i = [1,2], \tag{24}$$

hence, according to the Equations (19) - (24), the modified transfer matrix can be expressed as:

$$\boldsymbol{G'}_{2\times4} = \left[\begin{array}{cc|cc} 0 & 0 & 0 & 1 \\ 0 & 0 & 0 & 2 \end{array}\right], \tag{25}$$

Further details and in-depth mathematical description on the construction of the modified matrix construction can be found in [25], [37].

Let us now generalise the above-mentioned $\boldsymbol{G}_{2\times4}$ transfer matrix. Fig. 11 shows the transfer matrix $\boldsymbol{G}_{M\times(M+(K\times L))}$,[6] or $\boldsymbol{G}$ for brevity, which consists of two components. The first half is constituted by the identity matrix $\boldsymbol{I}_{M\times M}$, or $\boldsymbol{I}$ for short, which models the information frames' transmission from M SNs to the DN, and each of its entries is defined as:

$$I_{i,i} = \begin{cases} 1 & \text{if } I_{i,i} \text{ successfully recovered,} \\ 0 & \text{otherwise,} \end{cases} \tag{26}$$

[5] $\boxplus$ denotes the non-binary linear combination of the IFs, where all operations are carried out over GF [22].

[6] Here we assume single BP and CP, i.e. $n_1 = n_2 = 1$. However, the more general representation $\boldsymbol{G}_{n_1M\times(n_1M+n_2(K\times L))}$ would involve further concatenation of the matrix $\boldsymbol{G}_{M\times(M+(K\times L))}$ seen in Fig. 11.

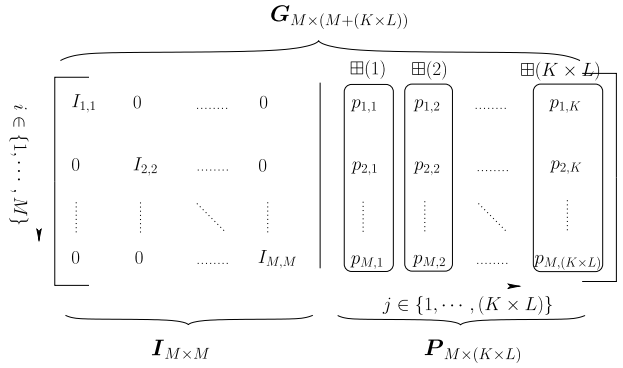

FIGURE 11. The generator matrix $G_{M\times(M+K)}$ characterising the NC transmission, where the notations are defined in Table 1.

where we have $i \in \{1, \cdots M\}$. The second component of $\boldsymbol{G}$ is the parity matrix $\boldsymbol{P}_{M\times(K\times L)}$, or $\boldsymbol{P}$ for short, which illustrates the PFs construction process formulated as:

$$\boxplus(j) = \boxplus\, p(i,j)I(i), \tag{27}$$

where we have $j \in \{1, \cdots (K \times L)\}$. Again, K and L denotes the number of the RNs and transmit antennas employed by each RN, respectively. Here, again, $\boxplus$ denotes the non-binary linear combination of the IFs over finite Galois Fields (GF) [22] which can be replaced with simple modulo-2 addition operation $\oplus$ when considering binary combination. Additionally, at the j^{th} RN, the modified version of the parity matrix, namely $\boldsymbol{P'}_{n_1\, M\times n_2\, K}$ represents the IFs status of being recovered or not according to:

$$p'_{i,j} = \begin{cases} p_{i,j} & \text{if } I_{i,i} \text{ successfully recovered at RN}_j, \\ 0 & \text{otherwise.} \end{cases} \tag{28}$$

In a nutshell, the modified matrix $\boldsymbol{G}'$ is constructed by modifying the entries of the original matrix $\boldsymbol{G}$ according to Equation (26) and Equation (28).

B. NETWORK DECODER

Following our discussions on the NC encoder, this section considers at the NC decoder briefly. The motivated readers might like to refer to [25], and to the references therein for more details. Let us consider the NC-based $\boldsymbol{G}_{4\times8}$ scheme depicted in Fig. 12 relaying on the transfer matrix of Equation (55). Let us assume that the full transmission resulted in a modified matrix of:

$$\boldsymbol{G'}_{4\times8} = \left[\begin{array}{cccc|cccc} 0 & 0 & 0 & 0 & 0 & 0 & 3 & 0 \\ 0 & 0 & 0 & 0 & 0 & 0 & 7 & 0 \\ 0 & 0 & 1 & 0 & 0 & 0 & 6 & 1 \\ 0 & 0 & 0 & 0 & 0 & 0 & 3 & 2 \end{array}\right]. \tag{29}$$

As suggested by Fig. 11, The modified transfer matrix $\boldsymbol{G}'_{4\times8}$ can be partitioned into:

$$\boldsymbol{I'}_{4\times8} = \begin{bmatrix} 0 & 0 & 0 & 0 \\ 0 & 0 & 0 & 0 \\ 0 & 0 & 1 & 0 \\ 0 & 0 & 0 & 0 \end{bmatrix}, \tag{30}$$

$$\boldsymbol{P'}_{4\times8} = \begin{bmatrix} 0 & 0 & 3 & 0 \\ 0 & 0 & 7 & 0 \\ 0 & 0 & 6 & 1 \\ 0 & 0 & 3 & 2 \end{bmatrix}. \tag{31}$$

Let us now denote the IFs transmitted from both SNs of Fig. 12 during the two BPs as $\boldsymbol{X}_{4\times8} = \{I_1^1(1), I_2^2(1), I_1^3(2), I_2^4(2)\}$, which can be illustrated in matrix format using:

$$\boldsymbol{X}_{4\times8} = \begin{bmatrix} I_1^1(1) & 0 & 0 & 0 \\ 0 & I_2^2(1) & 0 & 0 \\ 0 & 0 & I_1^3(2) & 0 \\ 0 & 0 & 0 & I_2^4(2) \end{bmatrix}. \tag{32}$$

Then the signals received at the DN during the BPs and CPs are denoted by $\boldsymbol{Z}_{I',4\times8}$ and $\boldsymbol{Z}_{P',4\times8}$, respectively and are formulated as:

$$\boldsymbol{Z}_{I',4\times8} = \boldsymbol{X}_{4\times8}\boldsymbol{I'}_{4\times8}, \tag{33}$$
$$\boldsymbol{Z}_{P',4\times8} = \boldsymbol{X}_{4\times8}\boldsymbol{P'}_{4\times8}, \tag{34}$$

Since the DN knows $\boldsymbol{G}'_{4\times8}$, both $\boldsymbol{Z}_{I',4\times8}$ and $\boldsymbol{Z}_{P',4\times8}$ can be estimated according to Equation (33) and Equation (34) as:

$$\boldsymbol{Z}_{I',4\times8} = \begin{bmatrix} 0 & 0 & 3 & 0 \end{bmatrix}, \tag{35}$$
$$\boldsymbol{Z}_{P',4\times8} = \begin{bmatrix} 0 & 0 & 47 & 11 \end{bmatrix}. \tag{36}$$

More explicitly, the entries of the vector in Equation (35) are calculated as:

$$0\cdot I_1^1(1)+0\cdot I_2^2(1)+1\cdot I_1^3(2)+0\cdot I_2^4(2)=3 \Rightarrow I_1^3(2)=3. \tag{37}$$

Similarly, the entries of the vector in Equation (36) can be expressed as:

$$3\cdot I_1^1(1)+7\cdot I_2^2(1)+6\cdot I_1^3(2)+3\cdot I_2^4(2)=47, \tag{38}$$
$$0\cdot I_1^1(1)+0\cdot I_2^2(1)+1\cdot I_1^3(2)+2\cdot I_2^4(2)=11. \tag{39}$$

Substituting the results of Equation (37) into both Equation (38) and Equation (39), we arrive at:

$$3\cdot I_1^1(1)+7\cdot I_2^2(1)+3\cdot I_2^4(2)=29, \tag{40}$$
$$2\cdot I_2^4(2)=8 \Rightarrow I_2^4(2)=4. \tag{41}$$

Upon substituting Equation (41) into Equation (40), we arrive at:

$$3\cdot I_1^1(1)+7\cdot I_2^2(1)+3\cdot I_2^4(2)=29, \tag{42}$$
$$3\cdot I_1^1(1)+7\cdot I_2^2(1)=17. \tag{43}$$

Observe in Equation (43) that we only have a single equation, but two unknown variables. Hence, out of the four transmitted IFs, only two IFs namely $I_1^3(2)$ and $I_2^4(2)$ can be recovered based on Equation (37) and Equation (41), respectively.

To generalise, let us assume that $\boldsymbol{X}^s$ denotes the IFs transmitted by the SNs to both the RNs and the DN during the BP, while $\boldsymbol{X}^r$ represents the PFs transmitted from the RNs to the DN during the CP. This PF matrix is constructed using Equation (27). Then, upon using the modified matrices,

$\boldsymbol{P}'$ and $\boldsymbol{I}'$, the frames that are successfully received at the DN can be written as [25]:

$$\boldsymbol{Z}_{I'} = \boldsymbol{X}^s \boldsymbol{I}', \tag{44}$$

$$\boldsymbol{Z}_{P'} = \boldsymbol{X}^r \boldsymbol{P}', \tag{45}$$

where the matrices $\boldsymbol{Z}_{I'}$ and $\boldsymbol{Z}_{P'}$ denote the IFs and PFs that are successfully received at the DN during the BP and CP, respectively. Let us now assume that the DN can successfully recovers a set $\boldsymbol{X}^s_{I'}$ that is a correct subset of $\boldsymbol{X}^s$ and since the DN knows $\boldsymbol{G}'$ [17], [24], [38], i.e. the DN is aware of how each PF was constructed, $\boldsymbol{X}^s_{I'}$ is also a subset of $\boldsymbol{X}^r$. Thus, from Equation (44), we arrive at:

$$\boldsymbol{X}^s_{I'} = \boldsymbol{Z}_{I'} = \boldsymbol{Z}_{P'}. \tag{46}$$

Then, upon substituting Equation (46) into Equation (45) we arrive at [25]:

$$\left(\boldsymbol{X}^r - \boldsymbol{X}^s_{I'}\right) \boldsymbol{P}' = \boldsymbol{Z}_{P'} - \boldsymbol{X}^s_{I'} \boldsymbol{P}'. \tag{47}$$

Therefore, a set $\hat{\boldsymbol{X}}^s_{P'}$ of IFs may then be extracted from Equation (47) with the aid of the Gaussian elimination algorithm [38]. Consequently the entire set of the recorded IFs at the DN may be expressed as $\tilde{\boldsymbol{X}}^s_{P'} \cup \boldsymbol{X}^s_{I'}$ out of the full set $\boldsymbol{X}^s$ of IFs.

V. TRANSMISSION RATE AND DIVERSITY ORDER

Before detailing our adaptive scheme, let us remind the readers of our scenarios. Fig. 5 and Fig. 6 defined Scenario A and Scenario B, respectively. The main simulation parameters of both scenarios were listed in Table 3.

Again, the transmission structure employed can be divided into two layers, namely the FEC and NC layers. This section will discuss the transmission layer's rate as well as the overall system throughput.

A. TRANSMISSION RATE

Let us commence with the NC rate, which is directly related to the multiplexing versus diversity capability and it might be expressed as:

$$R_{DNC} = \frac{E\,[\#\text{ IFs from SNs}]}{E\,[\#\text{ IFs from SNs} + \#\text{ PFs -from RNs}]}, \tag{48}$$

where $E\,[\,]$ represents the expectation operation over the total number of simulated frames.

Naturally, when designing any cooperative scheme, we have to aim for reducing the number of PFs transmitted from the RNs during the CPs [38], without any performance degradation. As a further benefit of this reduction, the resources required, such as the time, bandwidth and power, for accomplishing a full transmission cycle might be reduced. Hence, for the same amount of available resources, the system might be able to admit more users or to transmit more IFs of the same number of users to the DN. One of the efficient techniques is to adaptively adjust the number of PFs depending on the prevalent to the channel quality. For the simplest non-adaptive case, the rate of Dynamic Network Coding (DNC) is given by:

$$R_{DNC} = \frac{n_1 \cdot M}{n_1 \cdot M + n_2 \cdot K \cdot L} \tag{49}$$

where M is the number of SNs and K is the number of RNs, while n_1 and n_2 represent the number of IFs and PFs, respectively. Recall that the parameters used in this paper are defined in Table 1, while the simulation parameters are listed in Table 3. When considering a single relay-aided Scenario A transmission, for example, the $R_{DNC} = 1/2$ BPS, where we have $M = 2$ SNs and $K = 1$ RN-aided $L = 2$ transmit antennas. Regarding the FEC layer used for direct transmission, without relaying, the effective FEC transmission rate R_{FEC} can be conventionally estimated using Equation (13). By contrast, the overall throughput of the relaying-aided DNC can be expressed as the number of information bits transmitted delivered by the number of modulated symbols transmitted during both phases [26]. More explicitly, the overall throughput of cooperative DNC can be formulated as:

$$\eta_{DNC} = \frac{n_1 \cdot M \cdot N_i}{n_1 \cdot M \cdot N_{BP} + n_2 \cdot K \cdot L \cdot N_{CP}}, \tag{50}$$

where N_i is the number of information bits per frame transmitted within a duration of $(N_{BP} + N_{CP})$ symbol periods and M denotes the number of users. Furthermore, N_{BP} is the number of modulated symbols per frame transmitted from the SNs during the BP, while N_{CP} is the number of modulated symbols per frame transmitted from the RNs during the CP. We have $N_{BP} = \frac{N_i}{R^{tx}_{\text{SN}}}$ and $N_{CP} = \frac{N_i}{R^{tx}_{\text{RN}}}$, where R^{tx}_{SN} and R^{tx}_{RN} denote the effective FEC transmission rates of the SN and RN, that can

TABLE 3. Simulation parameters for both Scenario A and Scenario B where the notations are defined in Table 1, while the rates corresponding to the $K = 1$ and $K = 2$ RN/RNs scenarios are summarised in Tables 4– 7, respectively.

Parameters	Scenario A Fig. 5	Scenario B of Fig. 6
Channel	(fast+slow) fading	(fast+slow) fading
TTCM coding rate	$R_{cm} = 1/2$	$R_{cm} = 1/2$
Puncturing rate	$R_p = 1$	$R_p = 1$
# symbols per frame	$N_s = 120\,000$	$N_s = 120\,000$
# simulated frame	100 000	100 000
Modulation	QPSK(BP/CP)	QPSK(BP) 16QAM-SPM(CP)
MUD types	ML	ML
Channel Access	2×2 (BP) 2×2 (CP)	2×1 (BP) 1×1 (CP)
Correlation coefficients $\rho =$	$\{0.8, 0.6, 0.2\}$	$\{0.8, 0.6, 0.2\}$
Number of SNs	$M = 2$	$M = 2$
Number of RNs	$K = \{1,\ 2\}$	$K = \{1,\ 2\}$
NC method	DNC/ADNC	DNC/ADNC
Transfer Matrix	$\boldsymbol{G}_{2\times4}$, $\boldsymbol{G}_{4\times8}$	$\boldsymbol{G}_{2\times4}$, $\boldsymbol{G}_{4\times8}$
Path-loss exponent	$\alpha = 2$	$\alpha = 2$

be estimated using Equation (13), respectively. Additionally, we assume having an identical number of BPs and CPs, i.e. $n_1 = n_2$. Thus, Equation (50) can be further simplified as:

$$\eta_{DNC} = \frac{M \cdot R^{tx}_{\mathrm{SN}} \cdot R^{tx}_{\mathrm{RN}}}{M \cdot R^{tx}_{\mathrm{RN}} + R^{tx}_{\mathrm{SN}} \cdot K \cdot L}, \tag{51}$$

hence, we have $\eta_{DNC} = 1$ BPS, when considering a single relay-aided Scenario A transmission associated with $M = 2$ SNs, $K = 1$ RN-aided $L = 2$ transmit antennas and FEC transmission rates of $R^{tx}_{\mathrm{SN}} = R^{tx}_{\mathrm{RN}} = 2$ BPS.

B. ADAPTIVE DYNAMIC NETWORK CODING

As suggested in the previous section, DNC-aided adaptive transmission is capable of enhancing the overall multiplexing or diversity gains. Similarly to the system proposed in [17], [26], in our ADNC system we assume that the DN has the capability of sending a feedback flag F_g back to the NC encoder of the RNs, as portrayed in Fig. 4. This flag requests the transmission of further PFs from the RNs during the BP according to the channel quality encountered. Intuitively, if the IFs were received correctly at the DN, then there is no need for any PF transmission. More explicitly, if the RNs received $F_g = 1$, this indicates that all IFs have been successfully decoded at the DN and hence the RNS become inactive. This adaptive operation may be formulated as:

$$(K_{\mathrm{AD}} \cdot L) = \begin{cases} 0 & \text{if } F_g = 1, \\ (K \cdot L) & \text{otherwise}, \end{cases} \tag{52}$$

where K_{AD} denotes the number of RNs used, while n_2 represents the number of the PFs sent from each RN. The corresponding adaptive NC rate might be expressed as:

$$R_{ADNC} = \frac{n_1 \cdot M}{n_1 \cdot M + E\left[n_2 \cdot K_{\mathrm{AD}} \cdot L\right]}, \tag{53}$$

where again, the expectation $E[\,]$ is evaluated over the number of simulated frames. Upon comparing Equations (52) with (53). For the case, when the number of SNs equals to that of NC the RNs, $M = K$, the adaptive NC rate of R_{ADNC} has to approach $\frac{n_1 \cdot M}{n_1 \cdot M} = 1$ for the sake of attaining the maximum achievable rate. Hence, in the high SNR region, i.e. when encountering a high channel quality or in highly correlated source scenarios, where the IFs can be recovered correctly during the BP, the term $K_{\mathrm{AD}} \cdot L$ has to be adaptively adjusted towards 0. For example, according to Equation (53) R_{ADNC} will assume two different values of $R_{ADNC} = 1$ BPS or ($R_{ADNC} = 1/2$) BPS if the feedback flag received $F_g = 1$ or (otherwise), when considering a single relay-aided Scenario A transmission associated with $M = 2$ SNs, $K = 1$ RN-aided $L = 2$. Upon assuming $n_1 = n_2$, similarly to Equation (51), the overall throughput of our adaptive scheme can be expressed as:

$$\eta_{ADNC} = \frac{M \cdot R^{tx}_{\mathrm{SN}} \cdot R^{tx}_{\mathrm{RN}}}{M \cdot R^{tx}_{\mathrm{RN}} + R^{tx}_{\mathrm{SN}} \cdot E\left[K_{\mathrm{AD}} \cdot L\right]}. \tag{54}$$

Similarly, $\eta_{ADNC} = 2$ BPS or ($\eta_{ADNC} = 1$) BPS according to whether the $F_g = 1$ or (otherwise), when considering a single relay-aided Scenario A transmission associated with $M = 2$ SNs, $K = 1$ RN-aided $L = 2$ transmit antennas and FEC transmission rates of $R^{tx}_{\mathrm{SN}} = R^{tx}_{\mathrm{RN}} = 2$ BPS.

C. DIVERSITY ORDER AND COMPLEXITY

In order to emphasise the scalability of our system, we consider a higher order transfer matrix of $\boldsymbol{G}_{4\times 8}$ that is constructed over GF(8), as follows [23], [24]:

$$\boldsymbol{G}_{4\times 8} = \left[\begin{array}{cccc|cccc} 1 & 0 & 0 & 0 & 3 & 7 & 3 & 6 \\ 0 & 1 & 0 & 0 & 5 & 7 & 7 & 4 \\ 0 & 0 & 1 & 0 & 2 & 4 & 6 & 1 \\ 0 & 0 & 0 & 1 & 5 & 5 & 3 & 2 \end{array}\right]. \tag{55}$$

As portrayed in Fig. 11, the NC transfer matrix $\boldsymbol{G}$ is comprised of two sub-matrices, namely the identity matrix $\boldsymbol{I}$ and the parity matrix $\boldsymbol{P}$. The sub-matrices of $\boldsymbol{G}_{4\times 8}$ in Equation (55) have two more columns and rows compared to those of $\boldsymbol{G}_{2\times 4}$ in Equation (14). Intuitively, this expansion can be exploited either by adding a pair of SNs and RNs, or by doubling the number of the BPs and CPs, respectively.

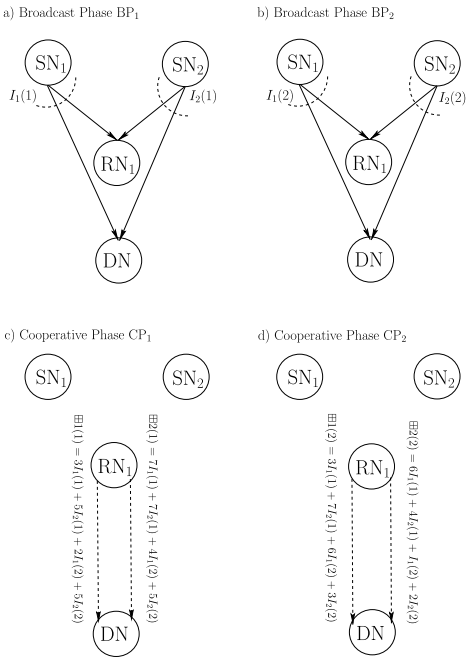

FIGURE 12. Schematic of the NC-based $G_{4\times 8}$-based system having $M = 2$ SNs, each transmitting $n_1 = 2$ IFs, while the $K = 1$ RN is equipped with $L = 2$ antennas that transmits $n_1 = 2$ IFs. The PFs transmitted during CPs, namely ⊞1(1), ⊞2(1), ⊞1(2) and ⊞2(2) are generated according to the 3rd, 4th, 5th and 6th columns of $G_{4\times 8}$, respectively, as specified in Equation (55). Table 1 defines the main system parameters.

In Fig. 12, we opted for the second option of increasing the number frames conveyed during the BPs and CPs, i.e. $n_1 = n_2 = 2$. For example, in Fig. 12 SN_1 broadcasts its IF I_1 twice, namely both within the first and in the second BPs as $I_1(1)$ and $I_1(2)$, respectively. Similarly, RN_1 sends the first PF ⊞1 as ⊞1(1) and ⊞1(2) during first and second CPs.

More explicitly, both the BP transmission slots can be illustrated by comparing the identity matrix of Equation (55)

to the upper part of Fig. 12, while the CPs can be characterised with the aid of the parity matrix of Equation (55) that is portrayed in the lower part of Fig. 12. The number of transmitted IFs and PFs is identical in $\boldsymbol{G}_{2\times4}$-based and the $\boldsymbol{G}_{4\times8}$-based scheme, i.e. we have $n_1 = n_2$. Hence, their NC rate will be the same as shown in Equation (49) Equation (53). However, the diversity order D_{NC} of the $\boldsymbol{G}_{4\times8}$-based scheme will be higher than that of its $\boldsymbol{G}_{2\times4}$-based counterpart [24]. Thus the diversity order D of the Dynamic Network Coding DNC-based system is bounded by [22], [24], [25], [37], [38]:

$$(K \cdot L) + n_2 \leq D_{DNC} \leq (K \cdot L) \cdot n_2 + 1, \tag{56}$$

where K is the number of RNs and L is the number of transmit antennas per RN, while we have $n_2 = 1$ or $n_2 = 2$ for the $\boldsymbol{G}_{2\times4}$ or $\boldsymbol{G}_{4\times8}$ based schemes, respectively. Naturally, a higher diversity order implies having a better Frame Error Ratio (FER) performance, since a higher diversity leads to an improved signal detection reliability. We considered a number of scenarios, each of which invoked either $K = 1$ RN or $K = 2$ RNs. The authors of [22], [24], [25], [37], [38] inferred the diversity order D_{DNC} in Equation (56) can be found using the following formula:

$$D_{DNC} = \lim_{\text{SNR}\to\infty} \frac{-\log_2 P_o}{\log_2 SNR}, \tag{57}$$

here the SNR is the signal to noise ratio, and P_o is the probability of erroneous frames that cannot be recovered at the DN. P_o can be approximated using $P_o = 1 - e^{(1-2^R)/SNR}$ and it has upper P_o^{Upper} and lower P_o^{Lower} outage bounds [38]. It was found in [25], [38], that the most influential variables in both P_o^{Upper} is $P_o^{(K\cdot L)\cdot n_2+1}$, and in P_o^{Lower} is $P_o^{(K\cdot L)+n_2}$, respectively. Thus, both upper and lower bounds are in-lined with the Equation (56). Note that the full derivation of P_o^{Upper} and P_o^{Lower} can be found in Equation (24) and Equation (28) of [25], respectively.

The corresponding rates and diversity orders are summarised according to the specific transfer matrix used in Tables 4–7. It can be clearly seen that, employing DNC schemes will increase the diversity order leading to a substantial performance improvement.[7] Naturally, this improvement comes at the expense of more transmitted frames, hence, higher decoding complexity as well as an increased delay. However, in our scenarios, we consider a relatively small number of: SNs, RNs, IFs n_1, and PFs n_2 where both the decoding complexity and the delay are managable [23], [24]. Additionally, our scheme exhibits a high diversity order, hence a further increase will bring marginal benefit. On one hand, the DNC constitutes relatively simple operations [23], [24] as it has been discussed in Section IV. More specifically, the DNC can be seen as a linear block code, namely a Reed Solomon (RS), with Maximum Distance Separable (MDS) code condition [22], [24], [38], where efficient decoding methods are exist[8] [23], [24]. However, implementing DNC scheme for a large number of SNs, RNs, IFs and PFs may be impractical [23], [24]. Hence, we have also conceived the ADNC design where the RNs would adaptively transmit their corresponding frames depending on channel-quality that would lead to a significant complexity reduction, particularly for high-SNR region.

[7] A gain of 19.0 dB was attained after employing our DNC scheme when compared against its non-cooperative counterparts as illustrated in Fig. 14.

TABLE 4. Rates and diversity orders of the systems based on the transfer matrices $G_{2\times4}$ and $G_{4\times8}$, when employing Scenario A of Fig. 5 and the number of the RNs is $K = 1$. Note that the terminologies are defined in Table 1, while the main parameters are listed in Table 3.

Parameters [BPS]	Equation	Scenario A, $G_{2\times4}$	Scenario A, $G_{4\times8}$
R_{FEC}	(13)	2	2
R_{DNC}	(49)	1/2	1/2
R_{ADNC}	(53)	$\begin{cases} 1 & \text{if } F_g = 1\,, \\ 1/2 & \text{otherwise}\,, \end{cases}$	$\begin{cases} 1 & \text{if } F_g = 1\,, \\ 1/2 & \text{otherwise}\,, \end{cases}$
η_{DNC}	(50)	1	1
η_{ADNC}	(54)	$\begin{cases} 2 & \text{if } F_g = 1\,, \\ 1 & \text{otherwise}\,, \end{cases}$	$\begin{cases} 2 & \text{if } F_g = 1\,, \\ 1 & \text{otherwise}\,, \end{cases}$
D_{DNC}	(56)	$3 \leq D_{DNC} \leq 3$	$4 \leq D_{DNC} \leq 5$
D_{ADNC}	(56)	$\begin{cases} 1 & \text{if } F_g = 1\,, \\ D_{DNC} & \text{otherwise}\,, \end{cases}$	$\begin{cases} 1 & \text{if } F_g = 1\,, \\ D_{DNC} & \text{otherwise}\,, \end{cases}$
n_1 [frame]	$--$	1	2
n_2 [frame]	$--$	1	2
M [user]	$--$	2	2

TABLE 5. Rates and diversity orders of the systems based on the transfer matrices $G_{2\times4}$ and $G_{4\times8}$, when employing Scenario B of Fig. 6 and the number of the RNs is $K = 1$. Note that the terminologies are defined in Table 1, while the main parameters are listed in Table 3.

Parameters [BPS]	Equation	Scenario B, $G_{2\times4}$	Scenario B, $G_{4\times8}$
R_{FEC}	(13)	3	3
R_{DNC}	(49)	1/2	1/2
R_{ADNC}	(53)	$\begin{cases} 1 & \text{if } F_g = 1\,, \\ 1/2 & \text{otherwise}\,, \end{cases}$	$\begin{cases} 1 & \text{if } F_g = 1\,, \\ 1/2 & \text{otherwise}\,, \end{cases}$
η_{DNC}	(50)	1.2	1.2
η_{ADNC}	(54)	$\begin{cases} 2 & \text{if } F_g = 1\,, \\ 1.2 & \text{otherwise}\,, \end{cases}$	$\begin{cases} 2 & \text{if } F_g = 1\,, \\ 1.2 & \text{otherwise}\,, \end{cases}$
D_{DNC}	(56)	$3 \leq D_{DNC} \leq 3$	$4 \leq D_{DNC} \leq 5$
D_{ADNC}	(56)	$\begin{cases} 1 & \text{if } F_g = 1\,, \\ D_{DNC} & \text{otherwise}\,, \end{cases}$	$\begin{cases} 1 & \text{if } F_g = 1\,, \\ D_{DNC} & \text{otherwise}\,, \end{cases}$
n_1 [frame]	$--$	1	2
n_2 [frame]	$--$	1	2
M [user]	$--$	2	2

[8] The transfer matrix can be derived from the appropriately selected systematic generator matrix $\boldsymbol{G}$ of an (n, k, d_{min}) linear block code [23], [24]. This linear block code should satisfy a Maximum Distance Separable (MDS) code condition for the sake of approaching the maximum distance bound [41]. In our work, we use the systematic generator matrix G of the Reed Solomon (RS) codes constituting a well-known and efficient class of MDS codes is provided by the software application SAGE [39].

TABLE 6. Rates and diversity orders of the systems based on the transfer matrices $G_{2\times4}$ and $G_{4\times8}$, when employing Scenario A of Fig. 5, while the number of RNs is $K = 2$. Note that the terminologies are defined in Table 1, while the main parameters are listed in Table 3.

Parameters [BPS]	Equation	Scenario A, $G_{2\times4}$	Scenario A, $G_{4\times8}$
R_{FEC}	(13)	2	2
R_{DNC}	(49)	1/3	1/3
R_{ADNC}	(53)	$\begin{cases} 1 & \text{if } F_g = 1\,, \\ 1/3 & \text{otherwise}\,, \end{cases}$	$\begin{cases} 1 & \text{if } F_g = 1\,, \\ 1/3 & \text{otherwise}\,, \end{cases}$
η_{DNC}	(50)	2/3	2/3
η_{ADNC}	(54)	$\begin{cases} 2 & \text{if } F_g = 1\,, \\ 2/3 & \text{otherwise}\,, \end{cases}$	$\begin{cases} 2 & \text{if } F_g = 1\,, \\ 2/3 & \text{otherwise}\,, \end{cases}$
D_{DNC}	(56)	$5 \le D_{DNC} \le 5$	$6 \le D_{DNC} \le 9$
D_{ADNC}	(56)	$\begin{cases} 1 & \text{if } F_g = 1\,, \\ D_{DNC} & \text{otherwise}\,, \end{cases}$	$\begin{cases} 1 & \text{if } F_g = 1\,, \\ D_{DNC} & \text{otherwise}\,, \end{cases}$
n_1 [frame]	$--$	1	2
n_2 [frame]	$--$	1	2
M [user]	$--$	2	2

TABLE 7. Rates and diversity orders of the systems based on the transfer matrices $G_{2\times4}$ and $G_{4\times8}$, when employing Scenario B of Fig. 6 and the number of RNs is $K = 2$. Note that the terminologies are defined in Table 1, while the main parameters are listed in Table 3.

Parameters [BPS]	Equation	Scenario B $G_{2\times4}$	Scenario B $G_{4\times8}$
R_{FEC}	(13)	3	3
R_{DNC}	(49)	1/3	1/3
R_{ADNC}	(53)	$\begin{cases} 1 & \text{if } F_g = 1\,, \\ 1/3 & \text{otherwise}\,, \end{cases}$	$\begin{cases} 1 & \text{if } F_g = 1\,, \\ 1/3 & \text{otherwise}\,, \end{cases}$
η_{DNC}]	(50)	0.86	0.86
η_{ADNC}	(54)	$\begin{cases} 2 & \text{if } F_g = 1\,, \\ 0.86 & \text{otherwise}\,, \end{cases}$	$\begin{cases} 2 & \text{if } F_g = 1\,, \\ 0.86 & \text{otherwise}\,, \end{cases}$
D_{DNC}	(56)	$5 \le D_{DNC} \le 5$	$6 \le D_{DNC} \le 9$
D_{ADNC}	(56)	$\begin{cases} 1 & \text{if } F_g = 1\,, \\ D_{DNC} & \text{otherwise}\,, \end{cases}$	$\begin{cases} 1 & \text{if } F_g = 1\,, \\ D_{DNC} & \text{otherwise}\,, \end{cases}$
n_1 [frame]	$--$	1	2
n_2 [frame]	$--$	1	2
M [user]	$--$	2	2

VI. PERFORMANCE RESULTS

The following two sections will discuss the performance results of Scenario A of Fig. 5 and Scenario B of Fig. 6, respectively. The main simulation parameters of both scenarios were listed in Table 3.

A. PERFORMANCE RESULTS OF SCENARIO A

The FER performance of the proposed DJSTTCM-aided DNC and ADNC schemes invoked in Scenario A is characterised in Fig. 13 and Fig. 14. It can be observed from all these FER performance results that our NC-aided schemes always perform better than the non-cooperative schemes, regardless of the correlation coefficient values. To elaborate further, Fig. 13 portrays the FER performance of Scenario A, when only a single RN ($K = 1$) is used, where the DJSTTCM-aided DNC/ADNC schemes are constructed

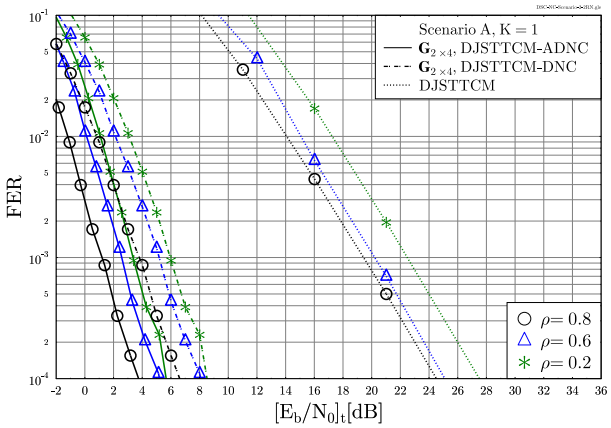

FIGURE 13. FER versus $[E_b/N_0]_t$ of the DJSTTCM-DNC/ADNC-aided $G_{2\times4}$ scheme of Fig. 4 in Scenario A, when $K = 1$ RN is invoked for various correlation coefficients. Note that the corresponding main simulation parameters are outlined in Table 3, while the associated variables are summarised in Table 4. The related results are summarised in Table 8.

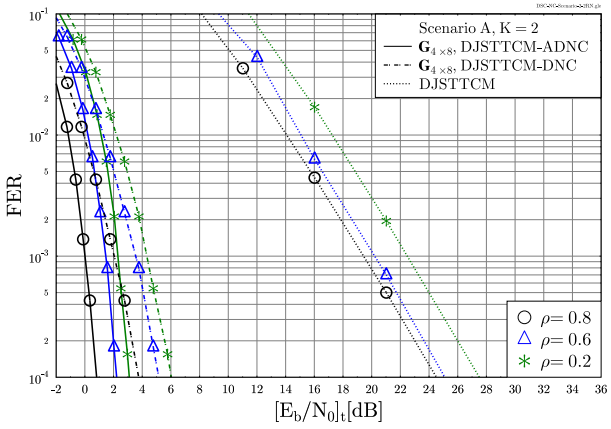

FIGURE 14. FER versus $[E_b/N_0]_t$ of the DJSTTCM-DNC/ADNC-aided $G_{4\times8}$ scheme of Fig. 4 in Scenario A, when $K = 2$ RNs is invoked for various correlation coefficients. Note that the corresponding main simulation parameters are outlined in Table 3, while the associated variables are summarised in Table 6. The related results are summarised in Table 8.

using the transfer matrix $\boldsymbol{G}_{2\times4}$ of Equation (14). As the figure shows, a substantial performance enhancement can be obtained, when employing our NC schemes benchmarked against its non-cooperative counterparts. More explicitly, at a FER level of 10^{-3} the DJSTTCM-ADNC scheme outperforms the DJSTTCM scheme by $[E_b/N_0]_t = 19.5 - 1.5 = 18.0$ dB for $\rho = 0.8$. This gain drops to $[E_b/N_0]_t \approx 14.7$ dB, when using the non-adaptive DJSTTCM-DNC scheme, as seen in Fig. 13. The adaptive feedback-flag based technique of Section V-B contributed a considerable $[E_b/N_0]_t$-performance improvement in comparison to that of the system operating without the adaptive mechanism. For example, an $[E_b/N_0]_t$-performance improvement of about 1.5 dB is recorded at an FER of 10^{-3}, when applying the adaptive feedback-flag based mechanism in the context of the DJSTTCM-ADNC for the $\boldsymbol{G}_{2\times4}$-based scheme relying on $\rho = 0.8$, as seen in Fig. 13.

Fig. 14 portrays the FER performance of our DJSTTCM-aided DNC/ADNC scheme of Fig. 4 using $K = 2$ RNs based

TABLE 8. System performance of the proposed DJSTTCM-DNC/ADNC scheme of Fig. 4 in Scenario A of Fig. 5 using simulation parameters of Table 3. The results are extracted from Fig. 13 and Fig. 14 at a FER level of 10^{-3}.

Scheme	p_e	ρ	Gain (dB)
DJSTTCM-DNC $G_{2\times4}$ Fig. 13	0.10	0.80	14.7
	0.20	0.60	14.6
	0.40	0.20	16.5
DJSTTCM-ADNC $G_{2\times4}$ Fig. 13	0.10	0.80	18.0
	0.20	0.60	17.4
	0.40	0.20	19.0
DJSTTCM-DNC $G_{4\times8}$ Fig. 14	0.10	0.80	17.5
	0.20	0.60	16.6
	0.40	0.20	18.0
DJSTTCM-ADNC $G_{4\times8}$ Fig. 14	0.10	0.80	19.5
	0.20	0.60	18.6
	0.40	0.20	20.0

on the $G_{4\times8}$ transfer matrix arrangement of Equation (55). As expected, employing a higher order transfer matrix improves the attainable performance further. For example, an impressive gain of about 19.5 dB is achieved when comparing the DJSTTCM-ADNC scheme to the DJSTTCM benchmark scheme for a correlation coefficient of $\rho = 0.8$. This performance improvement is an explicit benefit of the higher diversity gain offered by the $G_{4\times8}$-based arrangements over their $G_{2\times4}$-based counterparts. Similarly, applying our ADNC mechanism is expected to provide the scheme with a further $[E_b/N_0]_t$ gain. To elaborate, our adaptive DJSTTCM-ADNC schemes approach a FER $= 10^{-3}$ at 2 dB lower power than its non-adaptive DJSTTCM-DNC counterparts, as seen in Fig. 14. Table 8 summarises the attainable performance gains of our proposed schemes, namely of the DJSTTCM-DNC and DJSTTCM-ADNC, for Scenario A in comparison to the benchmark scheme dispensing with NC at an integrity requirement of FER $= 10^{-3}$.

Fig. 15 quantifies the schemes' effective per user throughput against SNR_t for our DJSTTCM-ADNC scheme, when employing $K = 1$ RN and $K = 2$ RNs. According to Equation (50) the non-adaptive schemes have an effective per user throughput of $\eta_{DNC} = 0.5$ [BPS], when a single RN is used. However this throughput is reduced to $\eta_{DNC} = 1/3$ [BPS], when adding one more RN, as shown in Fig.15(a) and Fig.15(b), respectively. As expected, upon invoking the ADNC scheme the overall normalised throughput, η_{ADNC}, increases when SNR_t increases. Hence, in the high-SNR_t region, more IFs may be recovered at the DN directly from the SNs, in which case $E[K_{\text{AD}}]$ of Equation (54) tends to zero. This implies that less PFs are required as SNR_t increases, where η_{ADNC} might asymptotically reach 1 BPS, which simply corresponds to the direct

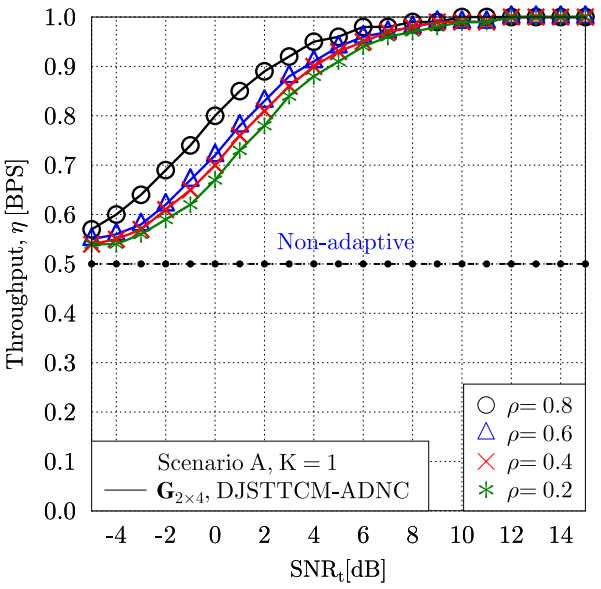

(a) $K = 1$ RN.

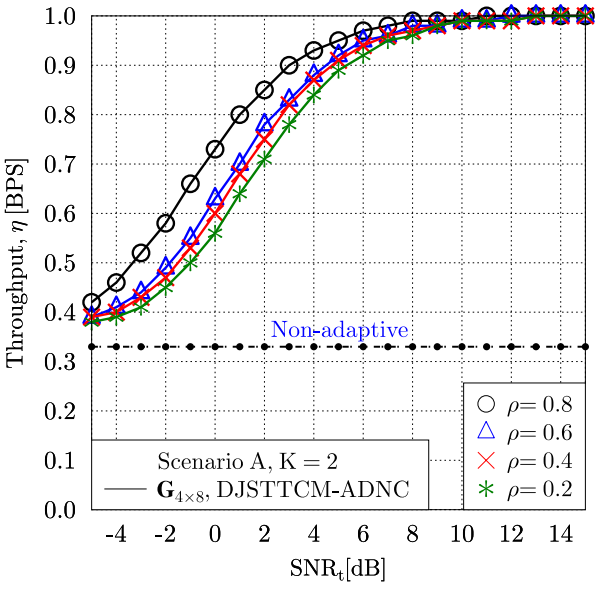

(b) $K = 2$ RNs.

FIGURE 15. Effective per user throughput versus transmit SNR of the DJSTTCM-ADNC when the Scenario A is invoked for various correlation coefficients. Note that the corresponding main simulation parameters are outlined in Table 3, while the associated rates of a) $K = 1$ RN and b) $K = 2$ RNs based schemes are summarised in Table 4 and Table 6, respectively.

link's rate computed from Equation (13). Note that, this would have a direct delay and decoding complexity reduction, as the number of number of PFs during the cooperative phase will be decreased. Therefore, Equation (54) implies that the effective throughput of the adaptive scheme, namely η_{ADNC}, exhibits a near-instantaneously time-variant nature, depending on the SNR of each transmission session.

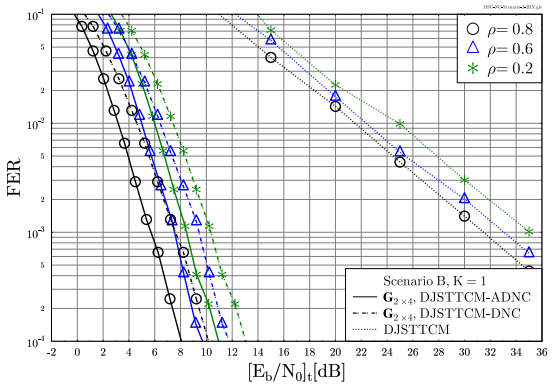

FIGURE 16. FER versus $[E_b/N_0]_t$ of the DJSTTCM-ADNC-aided $G_{2\times4}$ scheme of Fig. 4 in Scenario B, when $K = 1$ RN is invoked for various correlation coefficients. Note that the corresponding main simulation parameters are outlined in Table 3, while the associated variables are summarised in Table 5. The related results are summarised in Table 9.

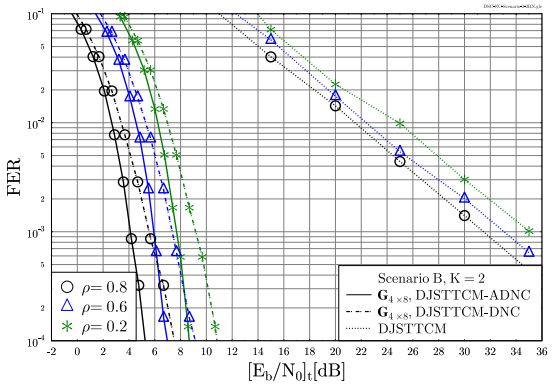

FIGURE 17. FER versus $[E_b/N_0]_t$ of the DJSTTCM-ADNC-aided $G_{4\times8}$ scheme of Fig. 4 in Scenario B, when $K = 2$ RNs is invoked for various correlation coefficients. Note that the corresponding main simulation parameters are outlined in Table 3, while the associated variables are summarised in Table 7. The related results are summarised in Table 9.

TABLE 9. System performance of the proposed DJSTTCM-DNC/ADNC scheme of Fig. 4 when the employing Scenario B of Fig. 6 and simulation parameters of Table 3 are used. The results are extracted from Fig. 16 and Fig. 17 when aiming for FER level of $= 10^{-3}$.

Scheme	p_e	ρ	Gain (dB)
DJSTTCM-DNC $G_{2\times4}$ Fig. 16	0.10	0.80	23.7
	0.20	0.60	23.5
	0.40	0.20	24.5
DJSTTCM-ADNC $G_{2\times4}$ Fig. 16	0.10	0.80	26.5
	0.20	0.60	25.2
	0.40	0.20	26.5
DJSTTCM-DNC $G_{4\times8}$ Fig. 17	0.10	0.80	26.0
	0.20	0.60	25.5
	0.40	0.20	25.5
DJSTTCM-ADNC $G_{4\times8}$ Fig. 17	0.10	0.80	27.4
	0.20	0.60	27.0
	0.40	0.20	27.2

When aiming for a fair comparison, using the SNR_t might be not suitable for a FER performance comparison. Thus, we have considered the transmit SNR per information bit

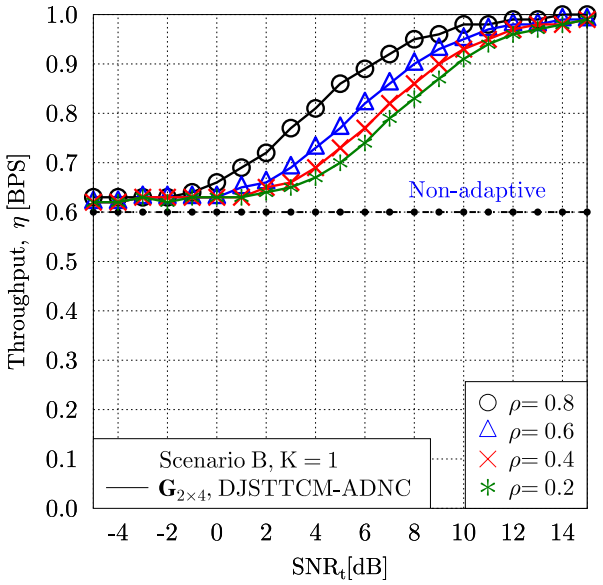

(a) $K = 1$ RN.

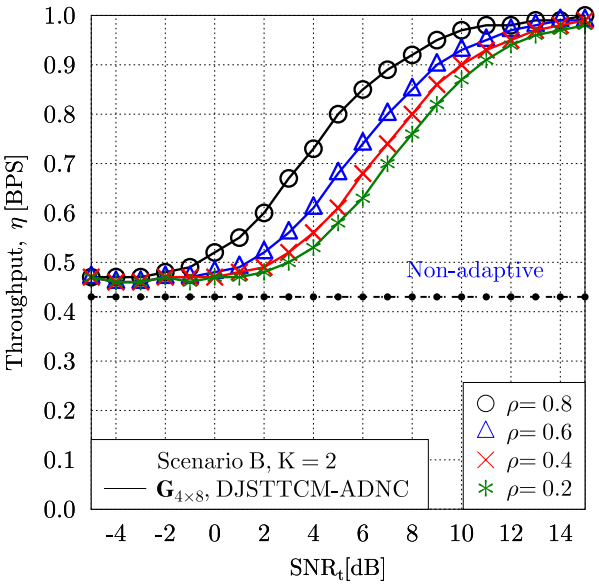

(b) $K = 2$ RNs.

FIGURE 18. Effective per user throughput versus transmit SNR of the DJSTTCM-ADNC when the Scenario B scenario is invoked. Note that the corresponding main simulation parameters are outlined in Table 3, while the associated rates of a) $K = 1$ RN and b) $K = 2$ RN based schemes are summarised in Table 5 and Table 7, respectively.

$[E_b/N_0]_t[\text{dB}] = \text{SNR}_t[\text{dB}] - 10\log_{10}(\eta_{ADNC})$, where the effect of the rate fluctuation has been eliminated.

B. PERFORMANCE RESULTS OF SCENARIO B

As the schematic of Fig. 6 shows, each node of our Scenario B arrangement, namely the SNs, RNs and the DN are equipped with a single transmit and/or receive antenna. This structure

constitutes an attractive scheme, especially when aiming for a reduced-complexity design, where each of the RNs combines both of the received IFs during the BP into a SPM signal [28].

Similar to Section VI-A, we will first discuss the FER performance of Scenario B, followed by its achievable throughput. As expected, the FER performance of Scenario A is better than that of Scenario B, since the MIMO structure of the former improves the system performance at the cost of a higher hardware complexity. However, our proposed scheme is still capable of outperforming the non-cooperative scheme for all the correlation values considered, as shown in Fig. 16 and Fig. 17. More quantitatively, our proposed DJSTTCM-ADNC-aided $\boldsymbol{G}_{2\times4}$ scheme of Fig. 4 requires only $[E_b/N_0]_t = 5.0$ dB to attain a FER $= 10^{-3}$, while the DJSTTCM dispensing with NC requires $[E_b/N_0]_t = 31.5$ dB at $\rho = 0.8$, as seen in Fig. 16. However, upon adding one more RN the proposed DJSTTCM-ADNC-aided $\boldsymbol{G}_{4\times8}$ only as 4.1 dB to achieve FER $= 10^{-3}$, as shown in Fig. 17. To summarise, Table 9 listed the FER performance of the DJSTTCM-DNC/ADNC schemes performance for Scenario B of Fig. 6.

Fig. 18 shows that the effective per user throughput increases as the SNR increases, when the adaptive scheme is activated. In contrast to Scenario A, the DJSTTCM-ADNC using $\boldsymbol{G}_{2\times4}$ requires almost $\text{SNR}_t = 14$ dB for asymptotically approaching a throughput of 1 BPS, as shown in Fig. 18(a). Otherwise similar trends prevail to those discussed in Section VI-B.

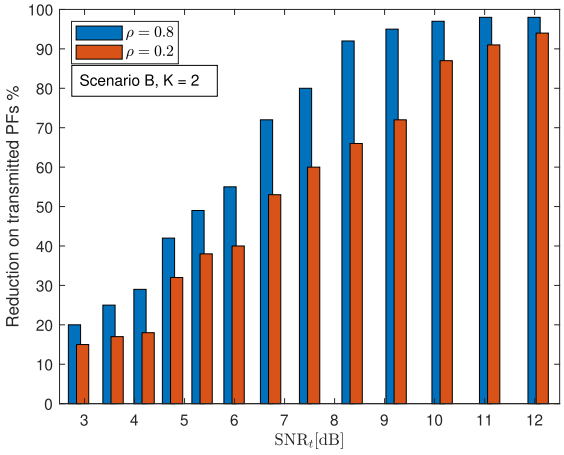

FIGURE 19. The reduction of the transmitted PFs during the cooperative phase when the Scenario B with $K = 2$ RN for $\rho = 0.8$ and $\rho = 0.8$ is invoked.

In order to investigate the decoding complexity reduction, we have analysed the complexity associated with the "DJSTTCM-ADNC" scheme for Scenario **B** with $K = 2$ RN, as shown in Fig. 19. Here the complexity reduction is quantified by determining the number of error-free IFs that can be recovered at the DN directly from the SNs. Hence, the RNs will avoid transmitting extra PFs that would be associated with significant decoding complexity. As Fig. 19 suggested, upon increasing SNR_t values the complexity reduced considerably as at $\text{SNR}_t = 10$ dB only 20% and 5% of the PFs are transmitted for $\rho = 0.2$ and $\rho = 0.8$, respectively.

VII. CONCLUSIONS

In this work the transmission of correlated source signals was assisted by two different NC schemes, which exhibited a robust performance for transmission over hostile channels. The BER performance of our cooperative arrangements was characterised when subjected to both uncorrelated Rayleigh fading and a quasi-static Rayleigh fading channels. A significant performance degradation was exhibited for transmission over quasi-static Rayleigh fading channels.

As a counter-measure, the use of both DNC and ADNC were conceived, where the time diversity between the frames will be further exploited. A substantial gain of 19.5 dB was attained at a correlation coefficient $\rho = 0.8$ over its counterpart dispensing with NC, as evidenced by Fig. 14.

Furthermore, according to the resources availability, two scenarios were considered. In Scenario A each of the RNs and the DN were equipped with two antennas, while in Scenario B, all RNs and the DN had a single antenna. Despite having only a single antenna in Scenario B, a robust performance was attained. Quantitatively, our DJSTTCM-ADNC scheme only requires $E_b/N_0 = 5.0$ dB and $E_b/N_0 = 4.1$ dB for achieving a FER of 10^{-3} by the $\boldsymbol{G}_{2\times4}$ and $\boldsymbol{G}_{4\times8}$ based schemes, respectively, as evidenced by Fig. 16 and Fig. 17.

ACKNOWLEDGMENT

The authors would like to thank DSR technical and financial support.

REFERENCES

[1] D. Slepian and J. Wolf, "Noiseless coding of correlated information sources," *IEEE Trans. Inf. Theory*, vol. IT-19, no. 4, pp. 471–480, Jul. 1973.
[2] Z. Xiong, A. D. Liveris, and S. Cheng, "Distributed source coding for sensor networks," *IEEE Signal Process. Mag.*, vol. 21, no. 5, pp. 80–94, Sep. 2004.
[3] J. Garcia-Frias, Y. Zhao, and W. Zhong, "Turbo-like codes for transmission of correlated sources over noisy channels," *IEEE Signal Process. Mag.*, vol. 24, no. 5, pp. 58–66, Sep. 2007.
[4] J. Garcia-Frias and Z. Xiong, "Distributed source and joint source-channel coding: From theory to practice," in *Proc. IEEE Int. Conf. Acoust., Speech, Signal Process. (ICASSP)*, Philadelphia, PA, USA, vol. 5, Mar. 2005, pp. 1093–1096.
[5] J. Garcia-Frias and Y. Zhao, "Near-Shannon/Slepian–Wolf performance for unknown correlated sources over AWGN channels," *IEEE Trans. Commun.*, vol. 53, no. 4, pp. 555–559, Apr. 2005.
[6] A. Wyner and J. Ziv, "The rate-distortion function for source coding with side information at the decoder," *IEEE Trans. Inf. Theory*, vol. IT-22, no. 1, pp. 1–10, Jan. 1976.
[7] J. Barros and S. D. Servetto, "Network information flow with correlated sources," *IEEE Trans. Inf. Theory*, vol. 52, no. 1, pp. 155–170, Jan. 2006.
[8] S. Gao, "Joint distributed source and network coding for correlated information multicasting," in *Proc. 6th Int. ICST Conf. Commun. Netw. China (CHINACOM)*, Harbin, China, Aug. 2011, pp. 698–702.
[9] T. Ho, M. Médard, and M. Effros, "Network coding for correlated sources," in *Proc. Conf. Inf. Sci. Syst. (CISS)*, Princeton, NJ, USA, Mar. 2004.
[10] O. Iscan, I. Latif, and C. Hausl, "Network coded multi-way relaying with iterative decoding," in *Proc. 21st Annu. IEEE Int. Symp. Pers., Indoor Mobile Radio Commun.*, Istanbul, Turkey, Sep. 2010, pp. 482–487.
[11] O. Iscan and C. Hausl, "Iterative network and channel decoding for the relay channel with multiple sources," in *Proc. IEEE Veh. Technol. Conf. (VTC Fall)*, San Francisco, CA, USA, Sep. 2011, pp. 1–5.

[12] F. P. S. Luus and B. T. Maharaj, "Joint source-channel-network coding for bidirectional wireless relays," in *Proc. IEEE Int. Conf. Acoust., Speech Signal Process. (ICASSP)*, Prague, Czech Republic, May 2011, pp. 3156–3159.
[13] Y. Wu, V. Stankovic, Z. Xiong, and S.-Y. Kung, "On practical design for joint distributed source and network coding," *IEEE Trans. Inf. Theory*, vol. 55, no. 4, pp. 1709–1720, Apr. 2009.
[14] J. Del Ser, P. M. Crespo, B. H. Khalaj, and J. Gutierrez-Gutuirrez, "On combining distributed joint source-channel-network coding and turbo equalization in multiple access relay networks," in *Proc. 3rd IEEE Int. Conf. Wireless Mobile Comput., Netw. Commun. (WiMob)*, White Plains, NY, USA, Oct. 2007, p. 18.
[15] X. Zhou, P.-S. Lu, K. Anwar, and T. Matsumoto, "Correlated sources transmission in orthogonal multiple access relay channel: Theoretical analysis and performance evaluation," *IEEE Trans. Wireless Commun.*, vol. 13, no. 3, pp. 1424–1435, Mar. 2014.
[16] P.-S. Lu, X. Zhou, and T. Matsumoto, "Outage probabilities of orthogonal multiple-access relaying techniques with imperfect source-relay links," *IEEE Trans. Wireless Commun.*, vol. 14, no. 4, pp. 2269–2280, Apr. 2015.
[17] H. V. Nguyen, S. X. Ng, and L. Hanzo, "Irregular convolution and unity-rate coded network-coding for cooperative multi-user communications," *IEEE Trans. Wireless Commun.*, vol. 12, no. 3, pp. 1231–1243, Mar. 2013.
[18] D. N. C. Tse and P. Viswanath, *Fundamentals of Wireless Communication*. New York, NY, USA: Cambridge Univ. Press, 2005.
[19] M. A. M. Izhar, A. J. Aljohani, S. X. Ng, and L. Hanzo, "Distributed joint source coding and trellis coded modulation for symbol-based Markov sources," *IEEE Trans. Veh. Technol.*, vol. 67, no. 5, pp. 4031–4041, May 2018.
[20] D. Elzouki, S. Dumitrescu, and J. Chen, "Lattice-based robust distributed source coding," *IEEE Trans. Inf. Theory*, vol. 65, no. 3, pp. 1764–1781, Mar. 2019.
[21] S. Kuhlmorgen, A. Festag, and G. Fettweis, "Exploiting distributed source coding for multi-hop routing in wireless ad hoc networks," in *Proc. IEEE 83rd Veh. Technol. Conf. (VTC Spring)*, May 2016, pp. 1–6.
[22] M. Xiao and M. Skoglund, "M-user cooperative wireless communications based on nonbinary network codes," in *Proc. IEEE Inf. Theory Workshop Netw. Inf. Theory*, Volos, Greece, Jun. 2009, pp. 316–320.
[23] J. L. Rebelatto, B. F. Uchôa-Filho, Y. Li, and B. Vucetic, "Generalized distributed network coding based on nonbinary linear block codes for multi-user cooperative communications," in *Proc. IEEE Int. Symp. Inf. Theory*, Austin, TX, USA, Jun. 2010, pp. 943–947.
[24] J. L. Rebelatto, B. F. Uchoa-Filho, Y. Li, and B. Vucetic, "Multiuser cooperative diversity through network coding based on classical coding theory," *IEEE Trans. Signal Process.*, vol. 60, no. 2, pp. 916–926, Feb. 2012.
[25] H. V. Nguyen, S. X. Ng, and L. Hanzo, "Performance bounds of network coding aided cooperative multiuser systems," *IEEE Signal Process. Lett.*, vol. 18, no. 7, pp. 435–438, Jul. 2011.
[26] W. Liang, H. V. Nguyen, S. X. Ng, and L. Hanzo, "Adaptive-TTCM-aided near-instantaneously adaptive dynamic network coding for cooperative cognitive radio networks," *IEEE Trans. Veh. Technol.*, vol. 65, no. 3, pp. 1314–1325, Mar. 2016.
[27] J. L. Rebelatto, B. F. Uchôa-Filho, Y. Li, and B. Vucetic, "Adaptive distributed network-channel coding," *IEEE Trans. Wireless Commun.*, vol. 10, no. 9, pp. 2818–2822, Sep. 2011.
[28] A. J. Aljohani, S. X. Ng, and L. Hanzo, "Distributed source coding and its applications in relaying-based transmission," *IEEE Access*, vol. 4, pp. 1940–1970, 2016.
[29] T. Ho, M. Medard, R. Koetter, D. R. Karger, M. Effros, J. Shi, and B. Leong, "A random linear network coding approach to multicast," *IEEE Trans. Inf. Theory*, vol. 52, no. 10, pp. 4413–4430, Oct. 2006.
[30] A. J. Aljohani, "Distributed joint source-channel coding and modulation for wireless communications," Ph.D. dissertation, Dept. Electron. Comput. Sci., Southampton Wireless Group, Univ. Southampton, Southampton, U.K., Dec. 2015.
[31] L. Hanzo, T. H. Liew, B. L. Yeap, R. Y. S. Tee, and S. X. Ng, *Turbo Coding, Turbo Equalisation and Space-Time Coding: EXIT-Chart Aided Near-Capacity Designs for Wireless Channels*, 2nd ed. Hoboken, NJ, USA: Wiley, 2011.
[32] A. J. Aljohani, S. X. Ng, R. G. Maunder, and L. Hanzo, "EXIT-Chart-Aided joint source coding, channel coding, and modulation design for two-way relaying," *IEEE Trans. Veh. Technol.*, vol. 62, no. 6, pp. 2496–2506, Jul. 2013.
[33] L. Kong, S. Xin Ng, R. G. Maunder, and L. Hanzo, "Maximum-throughput irregular distributed space-time code for near-capacity cooperative communications," *IEEE Trans. Veh. Technol.*, vol. 59, no. 3, pp. 1511–1517, Mar. 2010.
[34] H. Ochiai, P. Mitran, and V. Tarokh, "Design and analysis of collaborative diversity protocols for wireless sensor networks," in *Proc. IEEE 60th Veh. Technol. Conf. VTC-Fall*, Los Angeles, CA, USA, Sep. 2004, pp. 4645–4649.
[35] V. Toto-Zarasoa, A. Roumy, and C. Guillemot, "Maximum likelihood BSC parameter estimation for the Slepian-Wolf problem," *IEEE Commun. Lett.*, vol. 15, no. 2, pp. 232–234, Feb. 2011.
[36] K. Anwar and T. Matsumoto, "Accumulator-assisted distributed turbo codes for relay systems exploiting source-relay correlation," *IEEE Commun. Lett.*, vol. 16, no. 7, pp. 1114–1117, Jul. 2012.
[37] M. Xiao and M. Skoglund, "Multiple-user cooperative communications based on linear network coding," *IEEE Trans. Commun.*, vol. 58, no. 12, pp. 3345–3351, Dec. 2010.
[38] H. V. Nguyen, C. Xu, S. X. Ng, and L. Hanzo, "Non-coherent near-capacity network coding for cooperative multi-user communications," *IEEE Trans. Commun.*, vol. 60, no. 10, pp. 3059–3070, Oct. 2012.
[39] SAGE. *Open Source Mathematics Software*. Accessed: Aug. 8, 2015. [Online]. Available: http://www.sagemath.org/
[40] M. Xiao, J. Kliewer, and M. Skoglund, "Design of network codes for multiple-user multiple-relay wireless networks," *IEEE Trans. Commun.*, vol. 60, no. 12, pp. 3755–3766, Dec. 2012.
[41] C. Hausi and P. Dupraz, "Joint network-channel coding for the multiple-access relay channel," in *Proc. 3rd Annu. IEEE Commun. Soc. Sensor Ad Hoc Commun. Netw.*, Reston, VA, USA, vol. 3, Sep. 2006, pp. 817–822.

ABDULAH JEZA ALJOHANI (Member, IEEE) received the B.Sc. (Eng.) degree in electronics and communication engineering from King Abdulaziz University, Jeddah, Saudi Arabia, in 2006, and the M.Sc. degree (Hons.) and the Ph.D. degree in wireless communication from the University of Southampton, Southampton, U.K., in 2010 and 2016, respectively. He is currently an Assistance Professor with the Department of Electrical and Computer Engineering, King Abdulaziz University, Jeddah, Saudi Arabia. He is also associated with the Center of Excellence in Intelligent Engineering Systems. His research interests include joint source/channel coding, distributed source coding, coded modulation, channel coding, cooperative communications, and MIMO systems.

SOON XIN NG (Senior Member, IEEE) received the B.Eng. degree (Hons.) in electronic engineering and the Ph.D. degree in telecommunications from the University of Southampton, Southampton, U.K., in 1999 and 2002, respectively. He has been a member of academic staff with the School of Electronics and Computer Science, University of Southampton, since August 2006. From 2003 to 2006, he was a Postdoctoral Research Fellow working on collaborative European research projects known as SCOUT, NEWCOM, and PHOENIX. He is currently an Associate Professor of telecommunications with the University of Southampton. He has published over 250 articles. He has coauthored two John Wiley/IEEE Press books in his research field. He was involved in OPTIMIX and CONCERTO European projects as well as IU-ATC and UC4G projects. He was the Principal Investigator of an EPSRC project on cooperative classical and quantum communications systems. His research interests include adaptive coded modulation, coded modulation, channel coding, space-time coding, joint source and channel coding, iterative detection, OFDM, MIMO, cooperative communications, distributed coding, quantum communications, quantum error correction codes, and joint wireless-and-optical-fiber communications. He is a Chartered Engineer and a Fellow of the Higher Education Academy, U.K.